THE JOURNAL OF PHYSICAL CHEMISTRY B

Article

pubs.acs.org/JPCB

Water Dynamics in 1-Alkyl-3-methylimidazolium Tetrafluoroborate Ionic Liquids

Chiara H. Giammanco, Patrick L. Kramer, Daryl B. Wong, and Michael D. Fayer*

Department of Chemistry, Stanford University, Stanford, California 94305, United States

ABSTRACT: The effects of water concentration and varying alkyl chain length on the dynamics of water in 1-alkyl-3-methylimidazolium tetrafluoroborate room-temperature ionic liquids (RTILs) were characterized using two-dimensional infrared (2D IR) vibrational echo spectroscopy and polarization-selective IR pump−probe experiments to study the water hydroxyl (OD) stretching mode of dilute HOD in H_2O. Three imidazolium cation alkyl chain lengths, ethyl ($Emim^+$), butyl ($Bmim^+$), and decyl ($Dmim^+$), were investigated. Both $Bmim^+$ and $Dmim^+$ cations have sufficiently long chains that the liquids exhibit polar−apolar segregation, whereas the $Emim^+$ IL has no significant apolar aggregation. Although the OD absorption spectra are independent of the chain length, the measured reorientation and spectral diffusion dynamics are chain length dependent and tend to slow when the alkyl chain is long enough for polar−apolar segregation. As the water concentration is increased, a water-associated water population forms, absorbing in a new spectral region red-shifted from the isolated, anion-associated, water population. Furthermore, the anion-associated water dynamics are accelerated. At sufficiently high water concentrations, water in all of the RTILs experiences similar dynamics, the solvent structures having been fluidized by the addition of water. The water concentration at which the dilute water dynamics changes to fluidized dynamics depends on the alkyl chain length, which determines the extent and ordering of the apolar regions. Increases in both water concentration and alkyl chain length serve to modify the ordering of the RTIL, but with opposite and competing effects on the dissolved water dynamics.

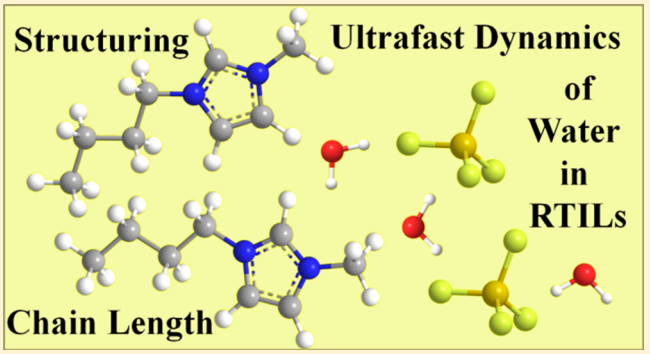

I. INTRODUCTION

Room-temperature ionic liquids (RTILs) are salts with melting points at or below room temperature due to their delocalized charge distributions, asymmetry, and flexibility, which impair crystallization.[1−3] There are a vast number of combinations of cations and anions that form ILs that have a wide range of properties.[2] They can be tuned to solvate both hydrophobic and hydrophilic moieties, have desirable electrochemical parameters, facilitate or forestall certain reactions, and stabilize certain reagents. RTILs have been proposed as "green" solvents for their typically low volatility and vapor pressure. Applications include batteries,[4−6] separations,[7,8] carbon capture,[9,10] and synthesis.[11−14]

One issue with incorporating ILs into processes is their high viscosities compared to molecular solvents. A possible solution is to mix the ILs with water (or another low-viscosity solvent) to decrease the viscosity but still maintain the properties of the IL.[15] However, the introduction of water can change the microscopic IL properties in addition to the bulk viscosity. Most RTILs are hygroscopic[16] and pick up non-negligible amounts of water from even short exposures to air unless they are kept in a dry atmosphere.[17] This amount of water alone is sufficient to alter viscosities and bulk properties.[13,18,19] The intentional introduction of additional water could cause dynamic and, at sufficiently high concentrations, structural changes.[20] Understanding the dynamics occurring in solution and how different water levels affect the behavior of ILs can be useful for tuning these systems for chemical applications.

In particular, the introduction of large amounts of water, instead of merely fluidizing the system, may cause structural changes. The local ordering of ILs has been the subject of many studies.[1,21−25] ILs have several types of ordering in solution, in addition to the adjacency correlations experienced by molecular solvents. The ions will arrange to maintain local charge neutrality, leading to a charge ordering. The RTILs can also exhibit polar−apolar ordering when there are sufficiently long alkyl groups present on the cations. These alkyl groups can aggregate to form apolar regions that can be relatively local or extended. Several studies have suggested that the threshold for the formation of this nonpolar region occurs at the 4-carbon butyl chain length.[1,24,26] As the alkyl chain length is increased, the apolar domains become larger, their correlation length typically scaling linearly with the alkyl chain length. This type of longer range ordering and the effect that it imparts on the dynamics of dissolved solutes are particularly intriguing to understand. Moreover, the effect of the introduction of water on the RTIL structures and their dynamics remains to be completely characterized.

Received: August 19, 2016
Revised: October 10, 2016
Published: October 11, 2016

DOI: 10.1021/acs.jpcb.6b08410
J. Phys. Chem. B 2016, 120, 11523−11538

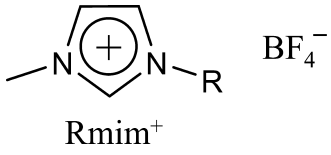

Figure 1. Structure of the 1-alkyl-3-methylimidazolium tetrafluoroborate ($RmimBF_4$) RTIL ions studied. In the present study, R = ethyl, butyl, octyl, or decyl.

1-Alkyl-3-methylimidazolium tetrafluoroborate ($RmimBF_4$) is a popular IL series, formed by altering the alkyl chain length on the cation (see Figure 1). This series has been the subject of previous studies investigating IL structuring,[24,27−30] and some works have focused on understanding the interaction with water.[20,31−35] These RTILs are fairly stable in air and water and not prohibitively viscous. The shorter chain lengths are completely miscible with water. By mixing varying amounts of water in this RTIL series, the effect of water on the dynamics and structure of the IL can be investigated. In the current study, we have investigated cations with alkyl chain lengths of R = E (ethyl), B (butyl), O (octyl), and D (decyl), labeled Emim, Bmim, Omim, and Dmim, respectively.

In the neat IL, there are weak hydrogen bonds formed between the cation and anion.[32] NMR studies have suggested that in $BmimBF_4$, from very low water concentrations and up to the 1:1 (ion pairs to water) concentration, the water binds to both cation and anion.[31] As the water is added, it acts as a hydrogen bond competitor with the cation for direct anion interactions and also disrupts the ring stacking, resulting in looser imidazolium−imidazolium interactions.[32] At lower water concentrations, this effect is localized, and water molecules sit in the preferential interaction sites of the anion. At higher water concentrations, the water begins to cluster and the incorporation of the clusters into the IL framework causes the structure to swell.[31] These observations are all for the butyl chain length; the present work will explore how the measured water dynamics reflect what is seen in the NMR data and how altering the chain length (and thus the amount of structuring in the IL) changes the nature of the trends supported by the previous NMR work. Simulations by Voth and co-workers suggested a breakdown of the alkyl region ordering with short chains near 1:3 ion pairs to water in BF_4 RTILs, which is not observed for longer chain lengths.[35]

In the following, FTIR absorption spectra, polarization-selective IR pump−probe experiments, and 2D IR spectroscopy are used to study the dynamics and structure of water in the $RmimBF_4$ series as a function of water concentration. The OD stretching mode of dilute HOD in H_2O is investigated to simplify the vibrational spectrum and eliminate vibrational excitation transport,[36,37] which interferes with the measurements. The pump−probe experiments were used to measure the vibrational energy relaxation lifetimes and the anisotropy decays (orientational relaxation). The 2D IR experiments measured spectral diffusion, which is related to the time-dependent frequency of the OD stretch. The range of frequencies within the inhomogeneously broadened absorption line is determined by the range of liquid structures. As the structure of the liquid evolves, the vibrational frequencies change from their initial values. Therefore, measurements of spectral diffusion report on the structural evolution of the systems.

II. EXPERIMENTAL METHODS

The ILs were purchased from IoLiTec, dried under vacuum while heating at 60 °C, and stored in a nitrogen atmosphere glovebox. Water was added to the IL, in the form of HOD (singly deuterated water) at 5 mol % in H_2O (resonant sample) or pure H_2O (nonresonant sample), by weight to attain the desired concentration. The concentrations will be reported as the mole ratio of IL ion pairs to water molecules (the total, including both H_2O and HOD). These concentrations were further verified through coulometric Karl Fischer titration. The solutions were sandwiched between 3 mm CaF_2 windows separated by a Teflon spacer. Absorption spectra were acquired using a Thermo Scientific Nicolet 6700 FTIR spectrometer. The spectra of the nonresonant samples were also taken, under identical conditions, and used to subtract the background.

The experiments (2D IR and IR pump−probe) were performed using a setup that has been described in detail previously.[38,39] Briefly, a 4 μm infrared laser pulse was split into either two (pump and probe for the polarization-selective pump−probe) or four (three excitation pulses and a local oscillator for the vibrational echo) replica pulses, whose variable timing was controlled with precision translation stages and focused to an approximately 100 μm spot in the sample. The resulting signal, collected in the appropriate phase-matched direction, was resolved by a monochromator configured as a spectrograph with a 150 line/mm grating and imaged by a 32 pixel mercury cadmium telluride array detector at each time delay of interest.

In the pump−probe experiment, a stronger pump pulse interacts to create a vibrational excited-state population in the sample, which is then probed after a specified waiting time by the weaker probe. The signal is obtained collinearly with the probe pulse. The pump pulse was polarized at 45° to the probe (horizontal), using a half-wave plate followed by a CaF_2 wire grid polarizer placed immediately before the sample to ensure purely linear polarization. The probe polarization was then resolved by a polarizer in a computer-controlled rotation stage following the sample and measured both parallel and perpendicular to the pump polarization. This scheme provides correctly normalized pump−probe decays in the two polarization configurations from which orientational anisotropy information was accurately extracted.

For 2D IR vibrational echo experiments, three pulses are directed into the sample in the box-CARS geometry with precisely controlled relative timing. The nonlinear vibrational echo signal is emitted following the third pulse in a distinct phase-matched direction. All pulses in this experiment were polarized parallel to each other (horizontal). After the sample, the emitted signal is overlapped spatially and temporally with the local oscillator pulse, with its timing and intensity controlled independently from the other pulses. The local oscillator enables heterodyne detection to retrieve phase information and amplify the weak signal.

III. RESULTS AND DISCUSSION

III.A. Linear Absorption Spectra. FTIR spectra were collected for the different chain length and water concentration samples for both 5% HOD solutions (resonant) and those made with pure H_2O (nonresonant). The nonresonant spectra were used to subtract the background to yield only the OD stretch absorption signal from the resonant samples. Figure 2A displays the spectra of solutions with a mole ratio of IL to water

DOI: 10.1021/acs.jpcb.6b08410
J. Phys. Chem. B 2016, 120, 11523−11538

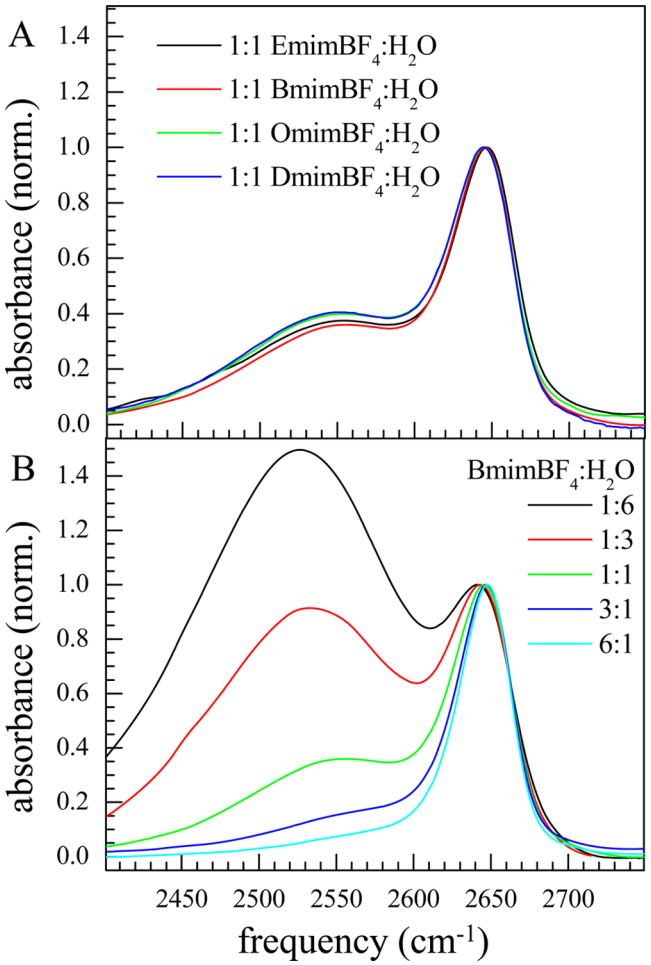

Figure 2. FTIR spectra of the OD stretch of dilute HOD in H_2O dissolved in ILs with the background (H_2O and IL) subtracted. (A) The effect of increasing the alkyl chain length for ~1:1 ion pair to water solutions. The 8-carbon alkyl chain IL 1-methyl-3-octylimidazolium tetrafluoroborate ($OmimBF_4$) is included along with the three ILs whose dynamics are studied. (B) The effect of increasing water concentration in $BmimBF_4$. As shown in (A), the water concentration series is similar for all chain lengths.

of 1 to 1. In addition to the 2-, 4-, and 10-carbon alkyl chain lengths examined in the rest of this article, the 8-carbon chain IL 1-methyl-3-octylimidazolium tetrafluoroborate ($OmimBF_4$) is included for comparison. The spectrum is essentially unchanged when the alkyl chain is elongated. The minor variations in the spectra are due to imperfect background subtraction and slight differences in concentration. Peak positions and widths are almost identical in the four solutions. This similarity of spectra with varying chain lengths persists at all water concentrations (not shown).

The second panel, Figure 2B, shows the effect of changing the amount of water. At low water concentration, there is essentially a single HOD population in solution that is centered around 2645 cm^{-1}. This is very blue-shifted from the spectrum of bulk water (centered at 2509 cm^{-1}),[40] which suggests that the water molecules form weaker hydrogen bonds on average than they would in the bulk. We attribute this peak to water donating hydrogen bonds to anions, a structural motif that is strongly supported by other linear and nonlinear IR studies of IL-solvated water[17,41,42] as well as molecular dynamics (MD) simulations.[43] As more water is added, a second population grows in on the red side of the spectrum. We attribute this band to a population of water hydroxyls that are engaged in hydrogen bonds with other water molecules.[17] This peak appears much closer to where bulk water absorbs, approaching the bulk water spectrum at high water concentration. The hydrogen bonds between water molecules are clearly stronger (shorter) than those with anions, producing a considerable redshift.[44] With the formation of a large enough water pool, the molecules will establish a hydrogen-bonding network, which will be indistinguishable from bulk water. However, the concentrations we are focusing on are well below this limit. Even though the hydroxyls are forming hydrogen bonds to other water molecules, these are not the same strength or necessarily the same geometry as found in bulk water. Thus, we expect the dynamics experienced by these water-associated water molecules to differ from those of both bulk water and water molecules that hydrogen bond with the BF_4^- anions.

From the absorption spectra, we can conclude that there are two separate populations in solution, one which increases in size with the addition of water relative to its blue-shifted counterpart. The spectra are independent of the alkyl chain length of the IL within experimental error. The spectra demonstrate that the water locates in the polar charged regions of the IL. The hydroxyl spectrum is mainly sensitive to the hydrogen bond strength and the very local environment of the hydroxyl. The results show that the hydrogen bond strength and the local environment of the HODs under observation are independent of the alkyl chain length. It is perhaps unsurprising that the effect of the growing nonpolar regions is minimal, given their hydrophobicity and unlikelihood to host the probed water molecules. However, it is interesting to note that in the short chain Emim liquid, the OD stretch has an identical spectrum as in the longer chain liquids, even though it does not have a sufficiently long chain to form a nonpolar region. Thus, the water spectrum does not depend on the size of the nonpolar region, and it does not apparently vary with the existence of some level of apolar aggregation. The spectra also indicate that increasing the chain length does not have a substantial effect on the structures of the ionic regions that give rise to the spectra.

The absorption spectrum is a very local property of the OD hydroxyl and its hydrogen bond. The invariance of the spectra to changes in the IL chain length does not imply that the dynamics experienced by the water molecules are identical in the various samples; time-resolved nonlinear IR experiments (Sections III.B–III.D) are needed to obtain this information. However, it does mean that it is reasonable to compare the same frequencies in the absorption spectra for samples with different chain lengths and know that differences in dynamics result from differences in motions and larger length scale structuring. The water molecules' local hydrogen-bonding environments for hydroxyls bound to anions are basically the same across chain lengths and water concentrations, though the exact motions in these environments can be perturbed by structural differences not reflected in the spectra.

III.B. Vibrational Relaxation. The average time for an excited vibration to transfer its energy to intra- or intermolecular (bath) modes is the vibrational relaxation time or lifetime. This time is the exponential decay time constant of an excited-state population relaxing to the ground state. The vibrational relaxation time is a very local quantity that depends on the coupling to intramolecular modes and to modes of the environment (bath).[45] If there are two separate populations in

DOI: 10.1021/acs.jpcb.6b08410
J. Phys. Chem. B 2016, 120, 11523−11538

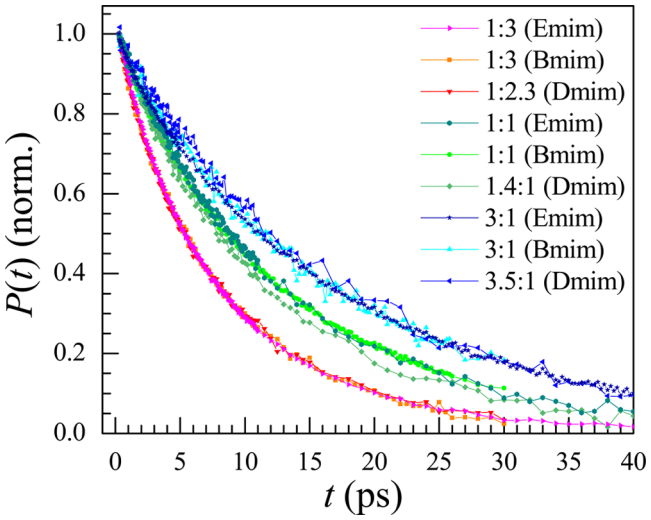

Figure 3. Population relaxation data (points) at the anion-associated water OD stretch peak wavelength for three different water concentrations and three different alkyl chain lengths. Similar concentrations are color coded such that the 1:3 ion pairs to water are represented in shades of red; 1:1, in green; and 3:1, in blue. The water concentration determines the decay rate(s), not the cation chain length.

solution with different local environments or intermolecular coupling, then generally there will be two vibrational lifetimes. The pump−probe lifetime measurement will yield a biexponential decay. A single exponential decay indicates a single population. However, it is possible, though unlikely, for two populations to accidentally have the same lifetimes. The lifetime is accessed by using polarization-selective pump−probe experiments.

The probe polarization following the sample is resolved parallel and perpendicular relative to that of the pump, to give the signals $S_{\parallel}(t)$ and $S_{\perp}(t)$, respectively. The normalized population relaxation, $P(t)$, is determined from the isotropic signal, which is free from the effects of rotation and is given by

$$P(t) = (S_{\parallel} + 2S_{\perp})/3 \quad (1)$$

Isotropic population decay data are shown in Figure 3 for the three IL solutions, $EmimBF_4$, $BmimBF_4$, and $DmimBF_4$, with various water concentrations.

At all water concentrations, there is a peak (~2645 cm^{-1}) that we have attributed to anion-associated hydroxyls via the linear spectra (Section III.A). At lower water concentrations, either this is the only population, or its peak wavelength is well separated from the relatively small water-associated peak. When the isotropic pump−probe signal (Figure 3) is observed near 2645 cm^{-1} in these low-water samples, a single exponential is sufficient to describe the decay curves, demonstrating that there is a single population of anion-associated hydroxyl. Note that at early times, a small-amplitude extra growth or decay appears, with sign and magnitude depending on the particular frequency position on the band. These features in the isotropic decay are caused by spectral diffusion, producing a net flow of population within the band. A nonequilibrium excited-state population can result from both nonuniform pumping caused by insufficient bandwidth of the pump or from a non-Condon effect causing the transition dipole moment magnitude to vary across the line, with larger values for stronger hydrogen bonds on the red side.[41,46] The center of the line is not greatly affected, but spectral diffusion is manifested as an extra decay on the red side and as a growth on the blue side as the nonequilibrium population relaxes via fast spectral diffusion from the overpumped red side of the line to the underpumped blue side. At the wavelengths observed, this effect has only a small-amplitude contribution. Fits to the curves with a single-exponential long-time population decay and an additional exponential for the short-time population spectral diffusion yield time constants for this spectral diffusion process that agree with the fastest time constant measured with the vibrational echo experiments and discussed in Section III.D. As this phenomenon has been documented and discussed in depth for other systems,[41] it will not be examined here further.

At higher water concentrations (ratio of less than or equal to 1:1), the vibrational population relaxation observed is best fit with a biexponential (in addition to the fast spectral diffusion). These concentrations have a significant water-associated hydroxyl (water−water) population, which gives rise to the broad band to the red of the anion-associated water peak. The water−water band overlaps the water−anion peak (Figure 2). Thus, two contributions to the population relaxation, $P(t)$, are expected, and the ratio of the amplitudes in the fits provides the population ratio at a given wavelength assuming that the transition dipoles of the two populations are equal at a particular wavelength. Independent of this assumption, the amplitude ratio provides exactly the relative signal contributions of the two populations, which are essential in determining the orientational relaxation parameters (Section III.C).

Comparing the vibrational relaxation for the different alkyl chain lengths for the anion-associated peak gives qualitatively similar results (Figure 3). Increasing the water concentration causes the lifetime to shorten. The presence of more bulklike water can alter the RTIL ionic region to provide more bath modes of appropriate energy for the anion-associated hydroxyl to relax into. But as mentioned previously, the vibrational relaxation is a very local property. Thus, given that all of the water in this peak is anion-associated, the effect of increasing the chain length and causing nonpolar aggregations to form is minimal. The hydroxyls are all directly bound to the tetrafluoroborate anion located in the ionic region, and the lifetime is determined by this very local interaction.

As is demonstrated in Figure 3, no chain length dependence is seen within error. The same concentrations (all taken at the anion-associated peak center) are colored in similar hues, such that the 1:3 ion pairs to water are shades of red, 1:1 are green, and 3:1 are blue. It is readily seen that a change in concentration alters the decays significantly but the cation chain length does not, as the results from the different chain lengths remain clustered. A full quantitative summary of the lifetimes, determined in the different solutions through biexponential fits that also take into account the fast population transfer, is given in Table 1.

The water-associated hydroxyl lifetimes can also be accessed for the higher concentrations where water-associated hydroxyls are present. Ideally, the lifetime would be able to be measured at the center of the water-associated band. However, these curves are more difficult to interpret, because there is spectral overlap with the higher level vibrational transition (1 to 2), which is shifted to the red by the anharmonicity of the vibration and is opposite in sign (see Section III.D). This places the 1 to 2 transition of the anion-associated peak squarely on top of the water-associated 0 to 1 peak and obscures the data. However, the water-associated lifetime is determined from the

DOI: 10.1021/acs.jpcb.6b08410
J. Phys. Chem. B 2016, 120, 11523−11538

Table 1. Summary of Vibrational Energy Relaxation Times from Biexponential Fits to the Isotropic Pump−Probe Decays[a]

solution	water−anion lifetime, T_1^a (ps)	water−water lifetime, T_1^w (ps)
6:1 $EmimBF_4$/water	19.1 ± 0.3	
6:1 $BmimBF_4$/water	16.9 ± 0.3	
3:1 $EmimBF_4$/water	17.9 ± 0.2	
3:1 $BmimBF_4$/water	17.7 ± 0.2	
3.5:1 $DmimBF_4$/water	17.5 ± 0.2	
1:1 $EmimBF_4$/water	13.4 ± 0.2	2.7 ± 0.1
1:1 $BmimBF_4$/water	14.4 ± 0.2	3.7 ± 0.1
1.3:1 $DmimBF_4$/water	13.2 ± 0.2	5.4 ± 0.3
1:3 $EmimBF_4$/water	9.4 ± 0.1	2.6 ± 0.1
1:3 $BmimBF_4$/water	9.3 ± 0.1	2.2 ± 0.1
1:2.3 $DmimBF_4$/water	10.1 ± 0.1	2.8 ± 0.1
1:6 $BmimBF_4$/water	7.7 ± 0.1	2.7 ± 0.1

[a]Error bars are standard deviations from the nonlinear fit.

biexponential fit in the regions of overlap between the two peaks. The two decaying exponentials are straightforward to assign to their respective populations because the amplitude of the water-associated contribution increases to the red side, whereas that of the anion-associated contribution increases to the blue. Furthermore, the anion-associated lifetime is typically substantially longer than that of the water-associated population. The lifetimes of both populations, water that is anion associated and water associated (when present), are given in Table 1.

At low water concentrations, there is only one population−water that is associated with anions. As the water content is increased, the second population of water-associated hydroxyls forms. Not only do these waters' hydroxyls have different hydrogen bond strengths leading to a different absorption spectrum, but they also have a different relaxation time from that of the anion-associated population. Thus, the water-associated hydroxyls (ODs) experience very different local environments and intermolecular couplings from the anion-associated water population. In the following Section III.C, it will be shown that these distinct populations also have different reorientation dynamics.

III.C. Orientational Relaxation. The polarization-selective pump−probe experiments provide details of the hydroxyl reorientation dynamics. The measured parallel and perpendicular signals are given by

$$S_{\parallel} = P(t)[1 + 0.8C_2(t)] \quad (2)$$

$$S_{\perp} = P(t)[1 - 0.4C_2(t)] \quad (3)$$

where $P(t)$ is the vibrational excited state population and $C_2(t)$ is the second-order Legendre polynomial orientational correlation function. By calculating the anisotropy, $r(t)$, the rotational dynamics are accessed

$$r(t) = \frac{S_{\parallel}(t) - S_{\perp}(t)}{S_{\parallel}(t) + 2S_{\perp}(t)} \quad (4)$$

For a single population of oscillators, the anisotropy is directly proportional to the orientational correlation function and simplifies to $r(t) = 0.4C_2(t)$, which is seen by inserting eqs 2 and 3 in eq 4. When multiple populations with different lifetimes are involved, a more complicated expression for the anisotropy is warranted. Equations 2 and 3 apply for each single population of oscillators; with multiple populations, the total parallel and perpendicular signals are the sums of eq 2 or 3 terms for each contributor. Because each population can reorient with different rates, there need to be two distinct orientational correlation functions. At each wavelength, both reorientational decays will contribute on the basis of the population ratio and weighted by their vibrational population decays, which are already known and are different (Section III.B).

The analysis of the HOD anisotropy curves starts at 280 fs for all of the chain lengths and concentrations. At shorter times, a nonresonant signal that tracks the pulse duration is present, which obscures the resonant OD stretch signal. Figure 4 displays anisotropy decays for HOD in $EmimBF_4$. The data for the other chain lengths are of similar shape and data quality (signal-to-noise ratios). Note that the curves extrapolated back to $t = 0$ do not achieve a $t = 0$ correlation value of 0.4. The difference between the extrapolated $t = 0$ point and 0.4 is caused by an ultrafast inertial motion, which occurs on a time

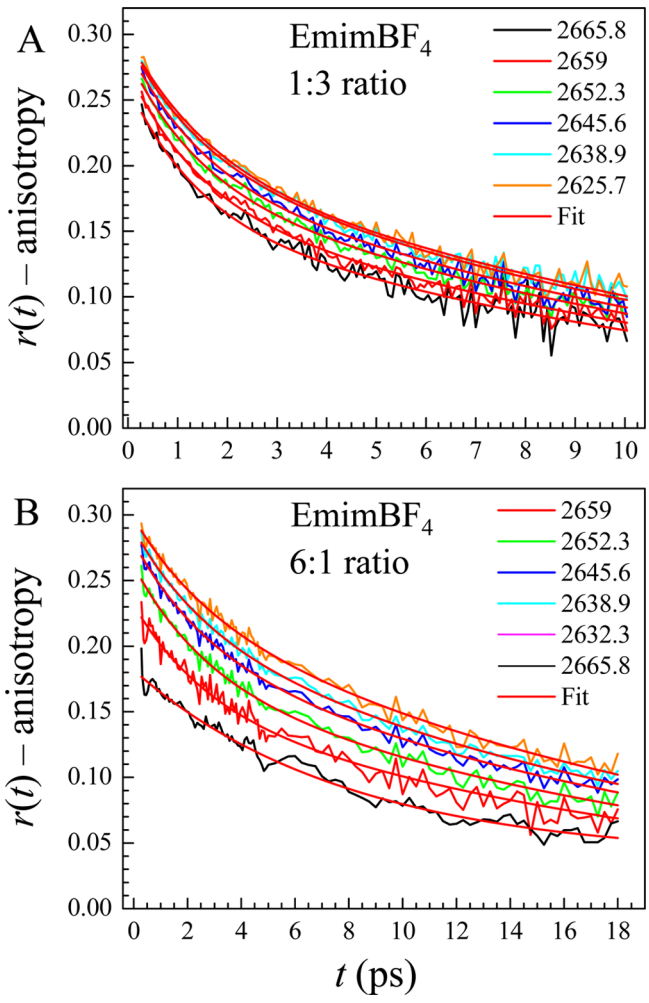

Figure 4. Representative curves for the anisotropy decays of the OD stretch of dilute HOD in H_2O in $EmimBF_4$ at different detection frequencies. (A) Concentrated solution, 1:3 $EmimBF_4/H_2O$. (B) Dilute solution, 6:1 $EmimBF_4/H_2O$. The fits to the curves using the appropriate form for the anisotropy decay (see text) are shown in red. The low water concentration, (B), is fit to the biexponential function, eq 6, whereas the presence of more water leads to two populations in solution in (A) and requires the full eq 5 to decompose the dynamics.

DOI: 10.1021/acs.jpcb.6b08410
J. Phys. Chem. B 2016, 120, 11523−11538

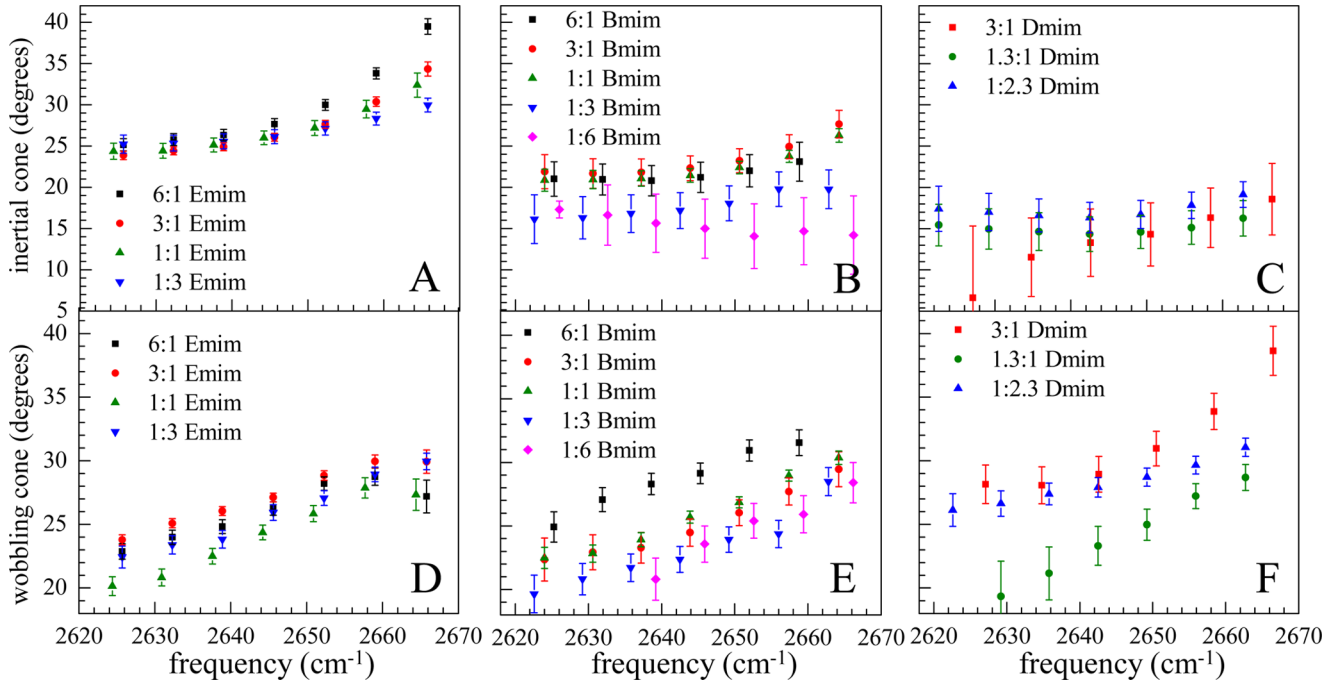

Figure 5. Plots of the cone half-angles for short-time restricted reorientation of the anion-associated hydroxyl in the RTIL solutions, from the wobbling-in-a-cone-analysis of anisotropy decays as a function of both detection frequency and water concentration. Top row (A–C): inertial cone angles. Bottom row (D–F): wobbling cone angles. The different chain length RTILs are grouped by column: A, D, $EmimBF_4$. B, E, $BmimBF_4$. C, F, $DmimBF_4$. Time constants are given in Table 2 for the wobbling cone, whereas the inertial cone reorientation occurs in <100 fs.[47]

scale less than 100 fs.[47] Even though we cannot assign a time constant to the inertial relaxation process, we do know its amplitude. This amplitude can be translated to an angular range of motion, as is discussed below, using a wobbling-in-a-cone analysis.[47−50] We will assume that both populations undergo the same amplitude of inertial motion at a particular wavelength because they are engaged in very similar strength hydrogen bonds, as indicated by having the same absorption frequency.[44,47]

To analyze the orientational dynamics, the data must be fit in the appropriate manner. When there is only one population present (low water concentrations), the anisotropy can be fit directly to extract the orientational correlation function. When there are two populations with different vibrational lifetimes, $r(t)$ is not free of population decay influence and the function can exhibit nonmonotonic behavior.[51] We must weigh the reorientation contribution from each population by the (normalized) population decay and the ratio of that population present at each wavelength; the resulting complete expression for the anisotropy is

$$r(t) = r_0\left[\frac{A\, e^{-t/T_1^w} R_w + (1-A)\, e^{-t/T_1^a} R_a}{A\, e^{-t/T_1^w} + (1-A)\, e^{-t/T_1^a}}\right] \quad (5)$$

Here, A is the fraction of the water-associated hydroxyl population with normalized orientational correlation function R_w; $(1-A)$ is the fraction and R_a is the orientational correlation function for the anion-associated population, and r_0 is an overall normalization factor. The lifetimes for the water-associated and anion-associated hydroxyl populations, T_1^w and T_1^a, respectively, as well as the fraction A at each wavelength, were determined from the population relaxation fits (Section III.B).

Within experimental error, the anisotropy decay of HOD in pure water is a single exponential with a time constant of 2.6 ps, following the ultrafast inertial component.[52,53] When in confined environments, the reorientation time of water can slow considerably.[51,54−56] In analogy with previous studies, we then model R_w as a single exponential decay, $R_w(t) = \exp(-t/\tau_{or}^w)$, with a single time constant to be determined, τ_{or}^w. A single exponential decay may also be used for R_a; however, this choice yields very poor fits to the measured anisotropy. When hydrogen bonded to an anion, water hydroxyls can undergo a wobbling motion on a faster time scale than that for complete orientational randomization, which typically involves breaking hydrogen bonds and undergoing angular jumps to new H-bond partners.[57,58] Without breaking the hydrogen bond, these anion-bound hydroxyls can nonetheless sample some range of angular space. Thus, they can experience a fast wobbling motion and a slower complete reorientation. To mathematically model these processes requires that R_a be biexponential

$$R_a(t) = B\exp(-t/t_1) + (1-B)\exp(-t/t_2) \quad (6)$$

where B is the fraction of the amplitude due to the faster wobbling motion and t_1 is its associated time constant, and t_2 is the time scale for the slower complete diffusive randomization. When there is no second (water-associated) population present, eq 5 reduces to eq 6 (multiplied by the scale factor r_0), which is completely free of population decay influence and can be used to fit the anisotropy directly. Otherwise, the anisotropy is fit with eq 6 inserted into eq 5 for the full model, determining the reorientation dynamics for both water-associated and anion-associated hydroxyl populations simultaneously. These fits produce excellent agreement with the experimental curves, as can be seen in Figure 4 for both high (Figure 4A) and low (Figure 4B) water concentrations in

DOI: 10.1021/acs.jpcb.6b08410
J. Phys. Chem. B 2016, 120, 11523−11538

$EmimBF_4$. The fit quality for intermediate water concentrations and the other two RTIL−water systems is very similar.

Once the fits are performed, the values for the water−water population orientational relaxation time and the long-time water−anion population reorientation time are known. For the shorter time constant corresponding to the wobbling motion, we utilize a wobbling-in-a-cone analysis, which models the restricted wobbling as free diffusion within a hard-walled cone.[48,50] The half-angle of the cone, θ_0, corresponds to the amplitude of the motion, or rather, how restricted the motion is. This is quantified through the order parameter,

$$S = \frac{\cos(\theta_0)(1 + \cos(\theta_0))}{2} \tag{7}$$

For the systems examined here, there are two cones overall: an initial fast inertial motion cone and the aforementioned wobbling cone.[59] These two restricted reorientation processes are taken to be independent of each other. Thus, the orientational correlation function is written as[48]

$$R_s(t) = (1 - S^2)\exp(-t(1/\tau^a_{wob} + 1/\tau^a_{or})) + S^2\exp(-t/\tau^a_{or}) \tag{8}$$

where τ^a_{or} corresponds to the reorientation time t_2, which was obtained using eq 6, and, by analogy between eqs 6 and 8, the expression for the wobbling time is readily found to be $\tau^a_{wob} = (1/t_1 - 1/\tau^a_{or})^{-1}$. Thus, by fitting the anisotropy, the final complete orientational randomization times for the two populations as well as the wobbling time of the anion-associated population are determined. The exponential amplitudes in the water−anion orientational correlation function, eq 8, yield the order parameter for the wobbling cone. The overall normalization constant r_0 in eq 5 is 0.4 times the order parameter for the inertial cone,[59] which is taken to be the same for both water populations at each wavelength. We first discuss the cone angles extracted from the fits to the anisotropy decays, which provide structural information on water's environment in the RTIL solutions through its effects on the hydroxyl angular potential. Next, with this knowledge in hand, we can analyze the timescales of both free and restricted orientational diffusion experienced by water that is associated with other water molecules or with anions.

The analysis of the restricted orientational relaxation cones can explicate how changes in chain length and water content affect the confining potential of water hydroxyls on short timescales, before they are able to randomize their orientations completely. The inertial cone (both populations) and the wobbling cone (anion-associated water population) half-angles are displayed as a function of detection wavelength, IL, and water concentration in Figure 5. For the low-water-content samples, the pump−probe signal comes mainly from the anion-associated water molecules. At higher concentrations of water, the inertial component amplitude will have contributions from both anion- and water-associated hydroxyls. As mentioned above, however, the inertial angular potential for both populations on this ultrafast time scale should be similar: the hydrogen bond strengths and geometries are closely matched, as evidenced by the fact that the hydroxyls absorb at the same frequency. The vibrational frequency is a sensitive probe of these structural parameters.[47] Water in the short-chain-length $EmimBF_4$ IL solution has a large-amplitude inertial component (Figure 5A), corresponding to an average cone half-angle nearly twice as large as seen in the longer chain length RTILs (Figure 5B,C). There is much less restriction of water motions on the ultrafast time scale in $EmimBF_4$.

The inertial cone (Figure 5A−C) is to some extent dependent on wavelength, consistent with observations of hydroxyls in both bulk water and other ILs.[41,47] The shift of the hydroxyl stretch frequency to the blue is the result of weaker hydrogen bonds.[44] For $EmimBF_4$ (Figure 5A), the increase in angular range of the inertial cone as the frequency increases is clear. As the hydrogen bonds become weaker, the hydroxyls can sample a wider range of angles in their inertial motion.[47] In effect, this is equivalent to a larger angular free volume for weaker hydrogen bonds. As the alkyl chain length is increased, the frequency dependence of the inertial cone is weakened considerably. For the longer chain ILs, there may be a small angular dependence of the inertial cone angle outside of the error bars, but only at the lowest water concentrations. For the higher water concentrations, there is little wavelength dependence within experimental error for any of the chain lengths (Figure 5A−C). When the ionic regions are completely fluidized, the hydrogen bond strength does not greatly affect the extent of ultrafast inertial motion. The ionic region structure, which results in the inertial cone confining potential, is altered more with water addition in $EmimBF_4$ than in $BmimBF_4$ or $DmimBF_4$.

The wobbling cone angles (Figure 5D−F) show a wavelength dependence for all samples and water concentrations. The slope does not change greatly with water concentration, except for the highest water concentration in $DmimBF_4$, for which the slope is somewhat less. Thus, the range of wobbling motion always depends on the hydrogen bond strength. As the ionic region is fluidized by water addition, the ultrafast inertial motion becomes equally free across frequencies, but the slower wobbling motion, depending on the local ion position fluctuations, retains influence of the initial H-bond strength.

The wobbling cone angles are shifted somewhat higher or lower for different concentrations in $BmimBF_4$ (Figure 5E) and $DmimBF_4$ (Figure 5F), but these differences may not be significant rather originating in the error inherent in the complete anisotropy fit with eq 5. The average angles for all three ILs are about the same, near 26° at the water−anion population line center (Figure 2). Although the angular range of the wobbling motion is not greatly affected by water concentration, as shown below, the time scale is very sensitive, revealing some surprising distinctions between the three IL chain lengths.

Both the wobbling diffusion constant and cone angle determine the observed wobbling correlation time.[48] But as we have found that the cone angles (Figure 5D−F) are approximately the same for all samples, the trends in the wobbling time constants can be interpreted equally well as trends in the more fundamental (inverse) diffusion constant. The analysis of the wobbling and diffusive reorientation timescales can now be addressed.

The effect of water concentration on the hydroxyl anisotropy decay times is not as clear-cut as that seen for the vibrational lifetimes (Figure 3, Table 1). When water molecules reorient in the bulk liquid, they do not undergo a continuous diffusive motion but rather experience a series of jumps that involve switching hydrogen bonding partners, that is, jump reorientation.[57,58] Jump reorientation is a concerted process and the structure surrounding the reorienting hydroxyl influences its rate. When water is constrained in the low water concentration ionic regions studied here, the environment still plays a role in

DOI: 10.1021/acs.jpcb.6b08410
J. Phys. Chem. B 2016, 120, 11523−11538

the reorientation dynamics. Even nonpolar regions, which do not directly act to cage or constrain the water molecules from moving, can slow reorientation. The length of the alkyl chains can influence the structure and intrinsic dynamics of the ionic regions. The rate of ion fluctuations around their equilibrium positions can affect the water reorientation time because ion position fluctuations will modulate the hydroxyl jump probability on or between anions.[60] Even though the water resides and reorients in the ionic region of the ILs, the structure imposed by the presence (or absence) of nonpolar regions has an effect on the time scale of this motion.

The time constants for reorientation (the wobbling and diffusive motions) are plotted as a function of water mole fraction (f_w) for each of the IL systems in Figure 6. The values for the time constants, resulting from the global fits as described above, are collected in Table 2 for all of the concentrations and chain lengths studied. Table 2 includes the water mole fraction values corresponding to the ion pair to water ratios for easy reference.

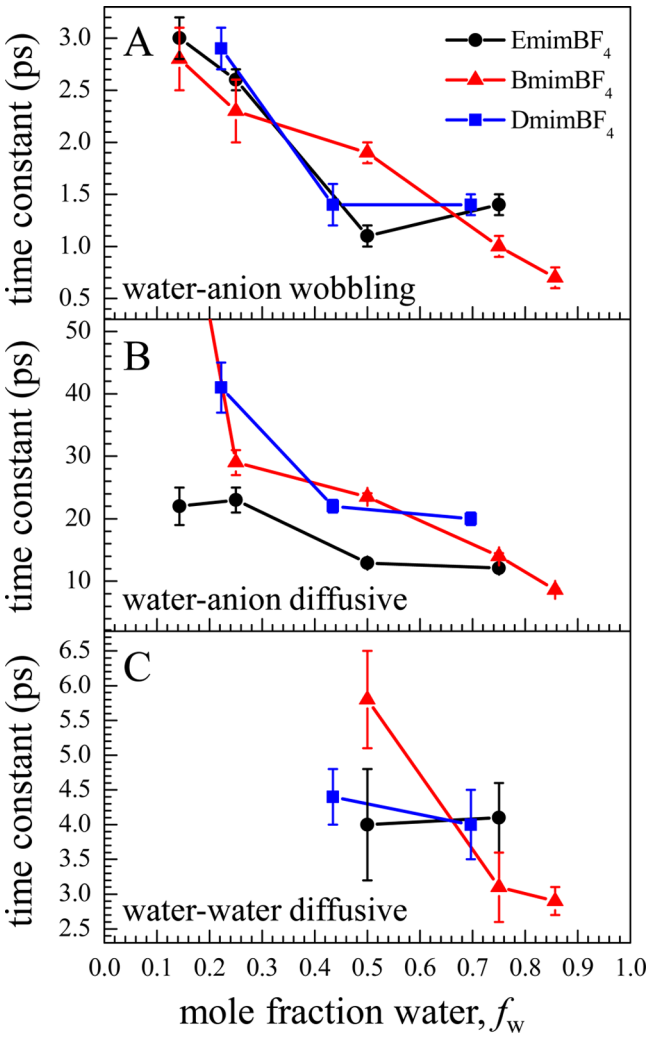

Figure 6. Time constants (points) for water hydroxyl reorientation in the RTIL solutions as a function of water mole fraction, f_w (correspondence to mole ratios given in Table 2). The lines are guides to the eye. (A) Wobbling-in-a-cone correlation time for anion-associated water. (B) Complete orientation randomization diffusion correlation time for anion-associated water. Note that the value for $BmimBF_4$ at mole fraction 0.14 (6:1 ion pairs to water) extends beyond the scale and is indicated by the line to the top of the panel. (C) Complete orientational randomization (diffusive) correlation time for the water-associated population of water.

There are two important regions of water content that will be discussed in turn. For mole fractions below 0.5 (1:1 ion pairs to water ratio), the water-associated population is too small for its contribution to the anisotropy to be obtained. Thus, only the reorientation dynamics of the anion-associated population are shown (Figure 6A,B). For $f_w \approx 0.5$ and above, there is an additional orientational relaxation time scale for the water-associated population (Figure 6C). The trends in time constants for the three RTIL−water systems differ in these two regimes as the water content is varied.

From the lowest water concentrations of 0.14 fraction to somewhat more at 0.25 (6:1 and 3:1 ratios, respectively), the wobbling time scale for all three RTIL solutions decreases similarly (Figure 6A). Toward a fraction of 0.5, the $EmimBF_4$ and $DmimBF_4$ solutions continue the trend and see a significant acceleration in the wobbling dynamics; this early-time component of the rotational motion has a similar time scale in both RTILs at all water concentrations. However, for the intermediate alkyl chain length system of $BmimBF_4$, the time constant only decreases moderately on approaching the 1:1 ion pair to water ratio. Contrary to the expectation that longer alkyl chain lengths increase the viscosity and thus slow the dynamics, at the 1:1 ratio water in the $BmimBF_4$ system wobbles more slowly than with either a shorter or longer alkyl chain length. For the longer-time-scale diffusive motion, which randomizes hydroxyl orientations, the trend is similar (Figure 6B). Water in the $EmimBF_4$ and $DmimBF_4$ solutions shows some acceleration in its diffusive reorientation between 0.25 and 0.5 water fractions, but in the $BmimBF_4$ solution the speedup is less. Thus, again, $BmimBF_4$'s time constant is longer than that of both of the other systems. This trend on varying the alkyl chain length with fixed water content is unexpected and indicates that there is some cooperativity between the structural changes because of increasing water content and chain length.

In the lower water regime, the ILs with the potential for intermediate range nonpolar ordering ($BmimBF_4$ and $DmimBF_4$) are distinguished from $EmimBF_4$ by the final diffusive reorientation time of anion-associated water. The time constant in $EmimBF_4$ does not change considerably between 0.14 and 0.25 fractions, but those for the longer chain ILs increase dramatically as the amount of water is decreased below $f_w = 0.25$. The $BmimBF_4$ value at 0.14 (or 6:1 ratio) is off the scale (which was chosen to emphasize the changes near 1:1 ratio). The line to the top of Figure 6B indicates the rapid change toward the 0.25 water fraction. Nonpolar aggregation thus dominates the IL ordering at low hydration levels, resulting in much slower dynamics.

In the higher water content regime, for water fractions of 0.5 and above, all three time constants are available in Figure 6. The results are similar in each anisotropy decay time scale for $EmimBF_4$ and $DmimBF_4$. After the more rapid changes below the 1:1 ratio point, the anion-associated water population's wobbling and diffusive motions plateau in time scale on going from 0.5 to 0.75 water fractions. The water-associated hydroxyl population does not change in its orientational diffusion time scale on increasing the water concentration. As with the lower water concentration range, $BmimBF_4$ solutions exhibit significantly different behavior. From 0.5 to 0.75 fraction and 0.75 to 0.86, the $BmimBF_4$ time constants in Figure 6 all

DOI: 10.1021/acs.jpcb.6b08410
J. Phys. Chem. B 2016, 120, 11523−11538

Table 2. Summary of Orientational Relaxation Times from Fits to the Anisotropy and Wobbling-In-a-Cone Analysis[a]

solution	f_w[b]	t_1 (ps)[c]	τ^a_{wob} (ps)[d]	τ^a_{or} (ps)[e]	τ^w_{or} (ps)[e]
6:1 $EmimBF_4$/water	0.14	2.7 ± 0.2	3.0 ± 0.2	22 ± 3	
6:1 $BmimBF_4$/water	0.14	2.7 ± 0.3	2.8 ± 0.3	79 ± 11	
3:1 $EmimBF_4$/water	0.25	2.3 ± 0.1	2.6 ± 0.1	23 ± 2	
3:1 $BmimBF_4$/water	0.25	2.2 ± 0.3	2.3 ± 0.3	29 ± 2	
3.5:1 $DmimBF_4$/water	0.22	2.7 ± 0.2	2.9 ± 0.2	41 ± 4	
1:1 $EmimBF_4$/water	0.50	1.1 ± 0.1	1.1 ± 0.1	12.9 ± 0.3	4.0 ± 0.8
1:1 $BmimBF_4$/water	0.50	1.7 ± 0.2	1.9 ± 0.1	23.5 ± 0.6	5.8 ± 0.7
1.3:1 $DmimBF_4$/water	0.44	1.3 ± 0.1	1.4 ± 0.2	22 ± 1	4.4 ± 0.4
1:3 $EmimBF_4$/water	0.75	1.2 ± 0.1	1.4 ± 0.1	12.1 ± 0.3	4.1 ± 0.5
1:3 $BmimBF_4$/water	0.75	1.0 ± 0.1	1.0 ± 0.1	14.0 ± 0.5	3.1 ± 0.5
1:2.3 $DmimBF_4$/water	0.70	1.2 ± 0.1	1.4 ± 0.1	20 ± 1	4.0 ± 0.5
1:6 $BmimBF_4$/water	0.86	0.7 ± 0.1	0.7 ± 0.1	8.6 ± 0.2	2.9 ± 0.2

[a]Error bars are standard deviations from the nonlinear fit. [b]Mole fraction of water corresponding to the given ion pair to water ratio. [c]Anisotropy fast decay time constant. [d]Wobbling time constant obtained from t_1 after wobbling analysis. [e]Diffusive orientational decay time constants for hydroxyl OD anion-associated (a) and water-associated (w) populations.

decrease with significant slopes. There is a particularly dramatic speedup in the water−water population's orientational diffusion on going above the 0.5 water fraction sample. Whereas, overall, all three IL systems exhibit periods of slow and rapid acceleration in the orientational relaxation times as the water concentration is increased, the $BmimBF_4$ case is exceptional in that all of the changes are displaced to larger water concentrations than for both a shorter chain length and a longer chain length IL, $EmimBF_4$ and $DmimBF_4$, respectively. Water in the $EmimBF_4$ and $DmimBF_4$ samples plateaus in orientational relaxation times by about the 1:1 ion pair to water ratio point, but for $BmimBF_4$, the dynamics continue to accelerate even up to a water fraction of 0.86 (1:6 ratio).

The hydroxyls of the water−water population, once it is present in the liquid due to a sufficient water concentration (Figure 2), can reorient rapidly (Figure 6C) because the nearby water molecules are good acceptors for new hydrogen bonds. The reorientation mechanism is similar to that in bulk water, as discussed above, but the limited spatial extent of these water clusters means the dynamics are necessarily slower. These water−water diffusion timescales are uniformly much faster than the final orientational diffusion times for the water−anion population (Figure 6B). The water molecules in this population can only reorient by changing the local hydrogen bond configuration on a given anion or jumping to form a hydrogen bond with a different anion. The anion-associated water population begins to reorient faster as the water content increases because the fluidization of the RTIL ionic region structure by progressively larger water clusters speeds up structural fluctuations within the ionic region, which in turn increases the rate at which constraints on hydroxyl reorientation are released.

The establishment of a progressively larger water-associated water population as the overall water content is increased drives the change in water reorientation dynamics in the RTIL systems. As the water content is increased, the weak hydrogen bonds of the anion to the cation become displaced by the water hydroxyls.[32] No significant apolar structuring is present in $EmimBF_4$, in which the positive charge is spread over the entire cation including the two carbons of the ethyl group.[21,61] The alkyl chains have partial positive charge and are too short to aggregate. Thus, formation of water clusters of increasing size, which can directly disrupt and screen the continuous polar network of an RTIL,[62] is the sole source of rapid variations in structure and dynamics. The addition of water quickly fluidizes the $EmimBF_4$ solutions from low water content. At higher water concentrations, the ionic region structure, which is still maintained by the need for local charge neutrality, cannot become any more fluidized and thus, the reorientation time constants for hydroxyls adjacent to both anions and other water molecules stop changing.

With longer chain length ILs, $BmimBF_4$ and $DmimBF_4$, the alkyl chains can aggregate to form nonpolar regions of the IL. But the nature of this nonpolar structural contribution is quite different between the intermediate butyl chain length and the much longer decyl. $DmimBF_4$, which phase separates at high water concentrations, has extensive chain aggregation into extended apolar domains. This inhibits major restructuring beyond the initial sharp increase in fluidity upon the addition of small amounts of water. The $DmimBF_4$ polar region fluctuations are slower, as indicated by the water−anion final diffusive reorientation rates (Figure 6B), but the trend in all reorientation rates as the water concentration increases is very similar to that for $EmimBF_4$.

Although there is apolar aggregation, the $BmimBF_4$ solutions do not have large extended or continuous apolar domains; the smallest chain length that produces extended apolar domains is hexyl.[21,63−65] As water is accumulated in the ionic region, the alkyl chains can more freely reorganize than those in $DmimBF_4$ solutions. In MD simulations of a longer chain but more polar IL, 1-methyl-3-octylimidazolium nitrate, Jiang and Voth found that a certain range of water content resulted in a "turnover" in the apolar organization, which they associated with the formation of micellar structures, leading to the sharpest features in the radial distribution functions.[62] It is plausible that the apolar ordering, which is just possible in the intermediate alkyl chain length $BmimBF_4$ solutions, is enhanced by a turnover concentration of water. The increased rigidity thus causes the relatively slow acceleration in anion-associated water reorientation times on approaching 1:1 $BmimBF_4$ to water. Thus, on approaching 0.5 water fraction, the fluidization of the ionic region results in enhanced apolar aggregation. On increasing the water content further, the restructuring of the polar head groups is more extensive, breaking apolar structural organization and causing the reorientation rates of both anion-associated and water-associated populations of water to steadily increase.

DOI: 10.1021/acs.jpcb.6b08410
J. Phys. Chem. B 2016, 120, 11523−11538

III.D. Spectral Diffusion. Another dynamical observable is provided by the 2D IR experiments. When a hydroxyl (OD) stretch is initially excited, it is in a particular environment and absorbs at a particular frequency in the inhomogeneously broadened absorption spectrum. As the liquid structure and resulting interactions experienced by the hydroxyl change, the hydroxyl stretch samples other frequencies in the absorption spectrum that correspond to different structural configurations. The time dependence of the frequency is known as spectral diffusion. After a sufficiently long time, the vibration will have sampled all of the frequencies in the inhomogeneously broadened absorption band because it will have sampled all possible liquid structures that contribute to the inhomogeneous broadening. To quantify the timescales of the structural fluctuations, which lead to this randomization of the frequency across the inhomogeneous line, we employ the frequency−frequency correlation function (FFCF). The normalized FFCF is the joint probability that a vibrational oscillator with a particular frequency at $t = 0$ will still have the same frequency at a later time t, averaged over all initial frequencies.

In the 2D IR experiments, three time-ordered laser field interactions prepare a final state, which emits the vibrational echo signal. The first laser pulse labels the vibrational oscillators' initial frequencies and begins a coherence period. After a time τ, the second laser pulse ends the coherence period and stores the accumulated phase relationships in a population state, where spectral diffusion can occur. Following the waiting time T_w, the third pulse begins a second coherence period, t, during which the signal (vibrational echo) emission occurs. Interferograms are obtained by scanning τ at a fixed T_w, while heterodyne-detecting and frequency-resolving the nonlinear signal. The monochromator provides the axis ω_m (vertical axis in the 2D spectra), which is Fourier conjugate to t. A numerical Fourier transform is performed on the τ-dependent interferograms, yielding the ω_τ axis (horizontal axis). The result is a correlation plot with the initial oscillator frequency, ω_τ, on the horizontal axis and the final oscillator frequency, ω_m, on the vertical axis. As T_w is increased, there is more time for the structure of the liquid to evolve, producing an increased extent of spectral diffusion, which is manifested as a change in the shape of the 2D spectrum. In the experiments, the 2D IR spectra are taken over a range of T_w values, and the change in shape of the spectrum is analyzed as discussed below.

Representative 2D IR spectra for the 1:1 $EmimBF_4$ to water sample are shown in Figure 7. At the shorter waiting time of T_w = 0.5 ps (Figure 7, top), two positive on-diagonal (dashed line) bands are visible: the 0−1 transitions for the anion-associated hydroxyls at 2645 cm^{-1} and those for the water-associated hydroxyls at 2550 cm^{-1}. Below each 0−1 band is a negative band that results from the 1−2 transition, which is shifted to lower frequency along ω_m by the vibrational anharmonicity. Only the 1−2 transition for the anion-associated hydroxyl population is visible in the spectral range shown. At short waiting times, there is substantial correlation between the initial and final frequencies, so the 2D line shapes appear elongated along the diagonal. As the waiting time is increased to a relatively long value of T_w = 13 ps, two changes occur. First, because the water-associated hydroxyls have vibrational lifetimes much shorter than this 13 ps waiting time (Table 1), the lower frequency 0−1 band has vanished as the excited population has relaxed. Second, the 0−1 and 1−2 bands of the anion-associated hydroxyl population have become close to round, as the correlation between the initial and final frequencies is lost through spectral diffusion.

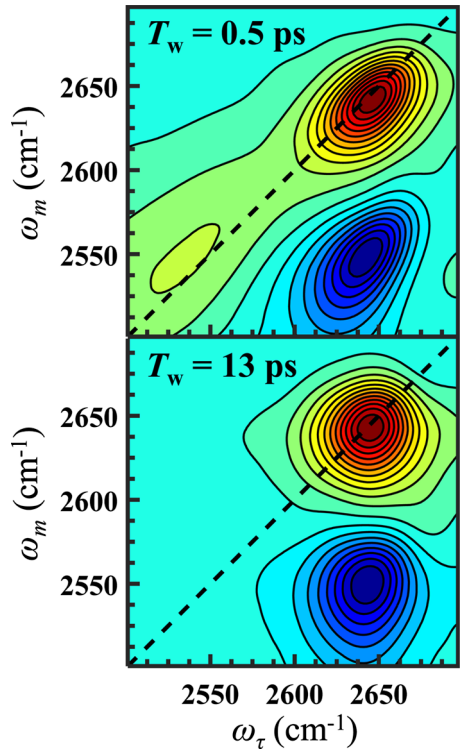

Figure 7. 2D IR spectra of the OD stretch of dilute HOD in H_2O in 1:1 $EmimBF_4$ to water, focusing on the anion-associated hydroxyl on-diagonal band centered at about 2645 cm^{-1}. Spectra at a short waiting time (top, T_w = 0.5 ps), showing a large amount of frequency correlation along the diagonal (dashed line), which is manifested as elongation along the diagonal, and a longer waiting time (bottom, T_w = 13 ps), after which a substantial amount of the correlation was lost, as indicated by the almost-round spectrum. The water-associated hydroxyl band (~2550 cm^{-1}) is redshifted sufficiently that it does not affect the center line slope (CLS) determination for the anion-associated band.

The normalized, T_w-dependent part of the FFCF is extracted from these correlation plots via the CLS method.[66,67] CLS values range from 1, for a band perfectly correlated along the diagonal, to zero, for an uncorrelated round band. The CLS decays as a function of waiting time for the different samples can be directly compared. Plots of the CLS analysis performed on the anion-associated peak are shown in Figure 8. The water-associated hydroxyl stretch peak could not be analyzed due to distortions arising from the 1 to 2 transition of the anion-associated peak (visible in Figure 7, top).

Several conclusions can be drawn from comparing the spectral diffusion of the anion-associated hydroxyls in the different chain length RTILs at a particular concentration. These appear in Figure 8A for the 1:3 ratio (1:2.3 for $Dmim^+$), Figure 8B for 1:1 (1.3:1 for $Dmim^+$), and Figure 8C for 3:1. For the highest water concentration (Figure 8A), the CLS decays are almost identical. This similarity in the decays suggests that, with a sufficient amount of water, the dominant structural fluctuations are not contingent upon the presence, absence, or extent of the nonpolar regions. As the concentration of water is decreased, the CLS decay for OD stretch of water in the short-chain $Emim^+$ solution does not slow as much as the decays for RTIL solutions with the longer alkyl tail cations. At the very low water concentration of 3:1 ion

DOI: 10.1021/acs.jpcb.6b08410
J. Phys. Chem. B 2016, 120, 11523−11538

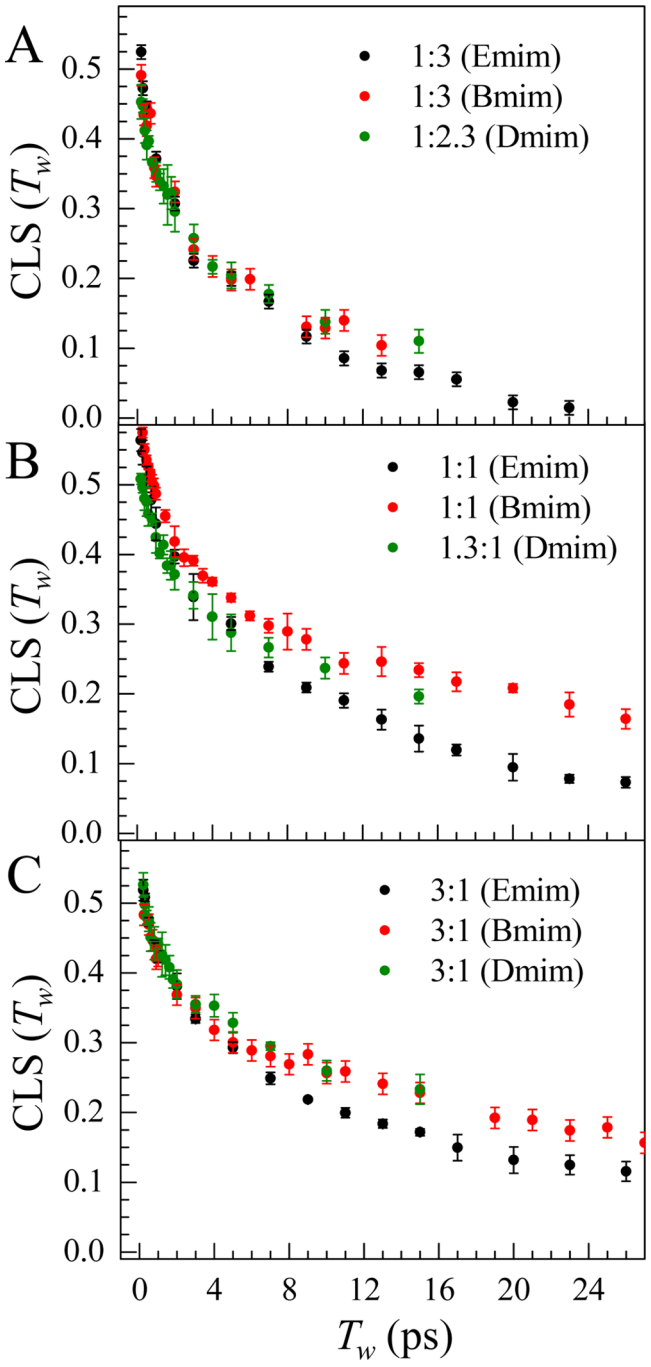

Figure 8. Plots of the extracted CLS decays vs the waiting time, T_w, for the anion-associated hydroxyls. The panels display different concentrations of water (listed as a ratio of ion pairs to water): (A) ∼1:3; (B) 1:1; and (C) 3:1. The different alkyl chain lengths of the cation are easily compared: $Emim^+$ (black), $Bmim^+$ (red), and $Dmim^+$ (green). At higher water concentrations (A), the structural fluctuations lead to very similar dynamics regardless of chain length. At lower water concentrations (B, C), it can be seen that the short-chain $Emim^+$ solutions undergo structural relaxation more quickly than the other two ILs that contain apolar regions. Data points are the average over multiple experiments, and error bars are the standard deviation.

pairs to water (Figure 8C), the longer chain length RTIL solutions exhibit very similar hydroxyl dynamics, distinct from those in the $EmimBF_4$ solution. Thus, it appears that the presence of a nonpolar region affects the dynamics water experiences, but the extent of the regions (which scales with the alkyl chain length) is less important in determining the fluctuation timescales.

To quantify the decays and the timescales of the fluctuations, the measured spectral diffusion (FFCF decay) can be modeled as a sum of exponentials. The complete FFCF can be written as

$$C(t) = \langle \delta\omega(t)\delta\omega(0)\rangle = \sum_i \Delta_i^2 \exp(-t/\tau_i) \quad (9)$$

where $\delta\omega(t) = \omega(t) - \langle\omega\rangle$ is the instantaneous frequency fluctuation. The structural fluctuations of the solution induce frequency fluctuations with amplitudes Δ_i and associated correlation times τ_i. If a component k has $\Delta_k\tau_k \ll 1$, then it is in the motionally narrowed limit, and Δ_k and τ_k cannot be determined independently. The motionally narrowed contribution to the FFCF is a component of the homogeneous pure dephasing, that is, it contributes to the homogeneous linewidth. The motionally narrowed contribution to the absorption spectrum has a pure dephasing linewidth given by $\Gamma^* = \Delta_k^2\tau_k/\pi = 1/(\pi T_2^*)$, where T_2^* is the pure dephasing time. The total homogeneous dephasing time that is measured, T_2, also depends on the orientational relaxation and vibrational lifetime, that is, $1/T_2 = 1/T_2^* + 1/(2T_1) + 1/(3T_{or})$. The full FFCF is obtained by fitting the CLS result in conjunction with the linear absorption spectrum of the vibrational probe. This enables the determination of the homogeneous contribution to the linewidth and the amplitudes of the FFCF components in frequency units, in addition to the time constants and relative amplitudes obtained directly from the CLS analysis.[66,67]

The CLS curves for the various samples all fit well to biexponential decay functions, indicating two major timescales of spectral diffusion. All of the CLS decays, along with biexponential fits, are shown in Figure 9. The biexponential fit time constants are summarized in Table 3, along with the amplitudes, Δ_i, and homogeneous linewidths, Γ, obtained from the FFCF fits. The fits are all in excellent agreement with the data (Figure 9, points). For comparison, the spectral diffusion of the OD stretch of dilute HOD in bulk water (H_2O) can also be fit to a biexponential with time constants of 0.4 ± 0.1 and 1.7 ± 0.1 ps.[68] In water, the fastest time scale (with about 60% contribution to the inhomogeneous linewidth) is ascribed to very local hydrogen bond length fluctuations, whereas the longer-time-scale decay is caused by the complete randomization of the hydrogen bond network. In the ILs, spectral diffusion of the anion-associated water hydroxyls occurs much more slowly than in bulk water. Water molecules are not part of a continuous H-bond network; rather, their nearest neighbors and H-bond acceptors are ions. Additionally, the much bulkier cations randomize their structures on considerably slower timescales,[20,69,70] which slows the environmental changes that are sensed by the water hydroxyls. Slowing of the spectral diffusion in aqueous salt solutions has been observed previously,[55] as well as in ILs.[41−43]

Figure 10 displays the faster (τ_1) and slower (τ_2) time constants from Table 3 as a function of the water mole fraction. For the highest water concentration studied, 1:6 $BmimBF_4$ to water ($f_w = 0.86$), there is a sizable water-associated population and the spectral diffusion (for the anion-associated population) is the fastest. The shortest spectral diffusion time constant for this concentration is the same as that found for HOD in bulk water,[71] whereas the slower time constant is ∼3 times slower than that found for bulk water (Figure 10, Table 3). This behavior is similar to spectral diffusion timescales seen in concentrated aqueous salt solutions.[55]

DOI: 10.1021/acs.jpcb.6b08410
J. Phys. Chem. B 2016, 120, 11523−11538

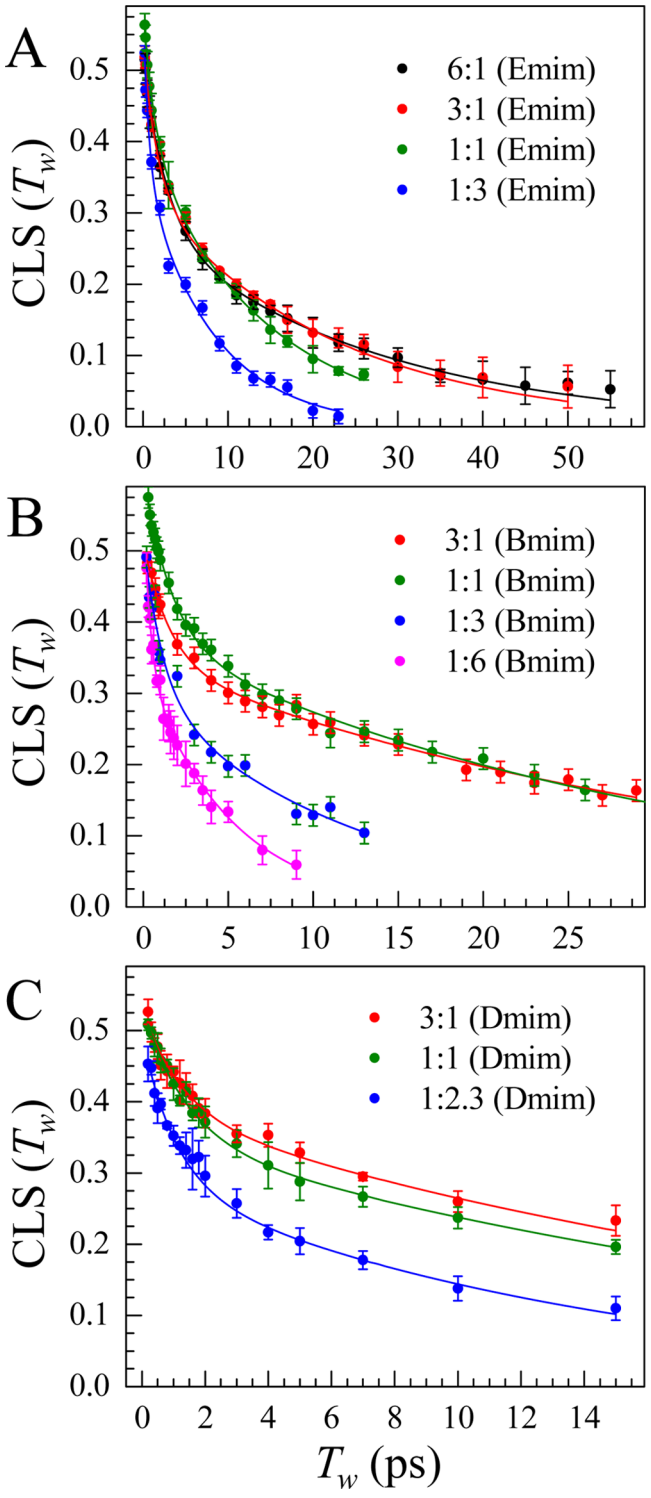

Figure 9. Plots of the CLS decays for the anion-associated hydroxyls in different alkyl chain length ILs: (A) $EmimBF_4$; (B) $BmimBF_4$; and (C) $DmimBF_4$. The data (points) are color coded by water concentration, expressed as the ratio of ion pairs to water molecules. Solid lines are biexponential fits to the data.

For all three chain length RTIL solutions, increasing the water concentration causes the spectral diffusion to accelerate. The water fraction dependence of the trend differs substantially between the faster component, τ_1 (Figure 10A), and the slower component, τ_2 (Figure 10B). At the lowest water fraction of 0.14 (6:1 $EmimBF_4$ to water), the fast spectral diffusion has a significantly longer time scale than in the three RTIL solutions with slightly more water, at a fraction of ~0.25 (3:1 ion pairs to water). The fluidization of the ionic region by the growth of water clusters has the most effect on these fastest structural fluctuations just as water clusters begin to form. On increasing to the 0.5 water fraction, there is no change in the faster time constants within the error (Figure 10A). With even more water, approaching a fraction of 0.75, the spectral diffusion is marginally accelerated by a similar amount for the three RTIL solutions. At each water concentration, the fast time constant is independent of chain length within experimental error. As mentioned above, on increasing the water content further to f_w = 0.86 for $BmimBF_4$, the fast time scale is more rapidly accelerated than around a 1:1 ratio, and it reaches the same value as for hydroxyls in bulk water.

The fast component arises from hydrogen bond length fluctuations similar to the fast component of HOD's spectral diffusion in bulk water.[43] It is a rapid motion depending on very local ion configurations around the hydroxyl. These are only appreciably altered when increasing the water content from a very dry RTIL (f_w = 0.14) or approaching rather large water fractions such as 0.86.

The slow component, shown as a function of water fraction in Figure 10B, has a different chain length dependence. When a sufficient amount of water is added to any of the three RTILs, it can disrupt the IL structure enough to alter the dynamics. At low water content, with water fractions between 0.14 and 0.25, the long-time-scale hydroxyl structural fluctuations in $BmimBF_4$ solutions are noticeably slower than those in $EmimBF_4$. For both of these IL solutions, the time scale steadily decreases with increasing water fraction. In the $DmimBF_4$ solutions, on the other hand, between f_w = 0.22 and 0.44, the slow spectral diffusion time constant does not change at all. The decyl chains are sufficiently long that apolar group aggregation can hold off on this transition from neat-IL-like dynamics to fluidized-IL dynamics. On increasing the water content further from the ~0.5 fraction to f_w = 0.75 (~1:3 ion pairs to water), the time constants in all three RTIL solutions are clearly approaching a similar value around 10 ps. $EmimBF_4$ and $BmimBF_4$ solutions are actually able to reach the same limit. For $DmimBF_4$, higher water concentrations lie past the saturation point of 1:2.3 ion pairs to water (f_w = 0.7). The structure established by the long alkyl tail chain lengths is so robust that the penalty for perturbing alkyl chain organization is very large. Rather than the alkyl chain arrangement being disrupted by larger water clusters in the ionic regions, which force a reconfiguration, the liquid does not allow the incorporation of more water and phase separation occurs.

The manner in which water influences $EmimBF_4$ and $BmimBF_4$ is fundamentally different from water's effects on $DmimBF_4$. $EmimBF_4$ and $BmimBF_4$ are completely miscible with water. Thus, as water is added, the RTIL liquid structure will continuously change to accommodate more and more water. For high enough water concentrations, these liquids will become water solvating relatively low concentrations of the anions and cations. $DmimBF_4$ has a structure that is more or less locked in by interactions leading to aggregation of the long alkyl chains, partitioning them away from the polar ionic groups.[1,25] Water molecules have to fit into this structure. Water influences the structure of the ionic regions, modifies the ionic region dynamics, and changes the overall bulk liquid dynamics.[20]

DOI: 10.1021/acs.jpcb.6b08410
J. Phys. Chem. B 2016, 120, 11523−11538

Table 3. Summary of FFCF Parameters from Fits to the Measured CLS Decays

solution	f_w [a]	Γ (cm^{-1}) [b]	Δ_1 (cm^{-1}) [b]	τ_1 (ps)	Δ_2 (cm^{-1}) [b]	τ_2 (ps)
6:1 $EmimBF_4$/water	0.14	18 ± 1	8.7 ± 0.7	2.7 ± 0.7	9.3 ± 0.6	27 ± 5
3:1 $EmimBF_4$/water	0.25	19 ± 1	8.1 ± 0.4	1.7 ± 0.5	10.2 ± 0.4	22 ± 4
3:1 $BmimBF_4$/water	0.25	19 ± 1	7.7 ± 0.3	1.5 ± 0.2	10.5 ± 0.2	36 ± 2
3.5:1 $DmimBF_4$/water	0.22	19 ± 1	6.9 ± 0.4	1.2 ± 0.2	11.0 ± 0.3	26 ± 4
1:1 $EmimBF_4$/water	0.50	17 ± 1	8.0 ± 0.2	1.5 ± 0.1	11.5 ± 0.2	14.3 ± 0.3
1:1 $BmimBF_4$/water	0.50	18 ± 2	8.0 ± 0.7	1.6 ± 0.3	11.0 ± 0.3	28 ± 3
1.3:1 $DmimBF_4$/water	0.44	19 ± 1	8.1 ± 0.4	1.3 ± 0.2	10.9 ± 0.3	26 ± 3
1:3 $EmimBF_4$/water	0.75	18 ± 1	8.7 ± 0.8	0.7 ± 0.4	10.7 ± 0.6	8.3 ± 1.1
1:3 $BmimBF_4$/water	0.75	18 ± 1	8.6 ± 0.4	1.1 ± 0.3	9.9 ± 0.4	12 ± 2
1:2.3 $DmimBF_4$/water	0.70	19 ± 1	8.2 ± 0.4	1.1 ± 0.3	9.9 ± 0.3	14 ± 2
1:6 $BmimBF_4$/water	0.86	19 ± 2	9.3 ± 0.5	0.4 ± 0.1	10.6 ± 0.2	5.0 ± 0.4

[a]Mole fraction of water corresponding to the given ion pair to water ratio. [b]The homogeneous linewidth $\Gamma = 1/(\pi T_2)$ is the FWHM of the Lorentzian contribution to the total linewidth, whereas the Δ_i's are standard deviations of the individual Gaussian inhomogeneous contributions. The total inhomogeneous linewidth (standard deviation) is $\sqrt{\Delta_1^2 + \Delta_2^2}$. The FWHM is 2.355 times the standard deviation. The total line shape is the convolution of the Lorentzian and the total Gaussian contributions.

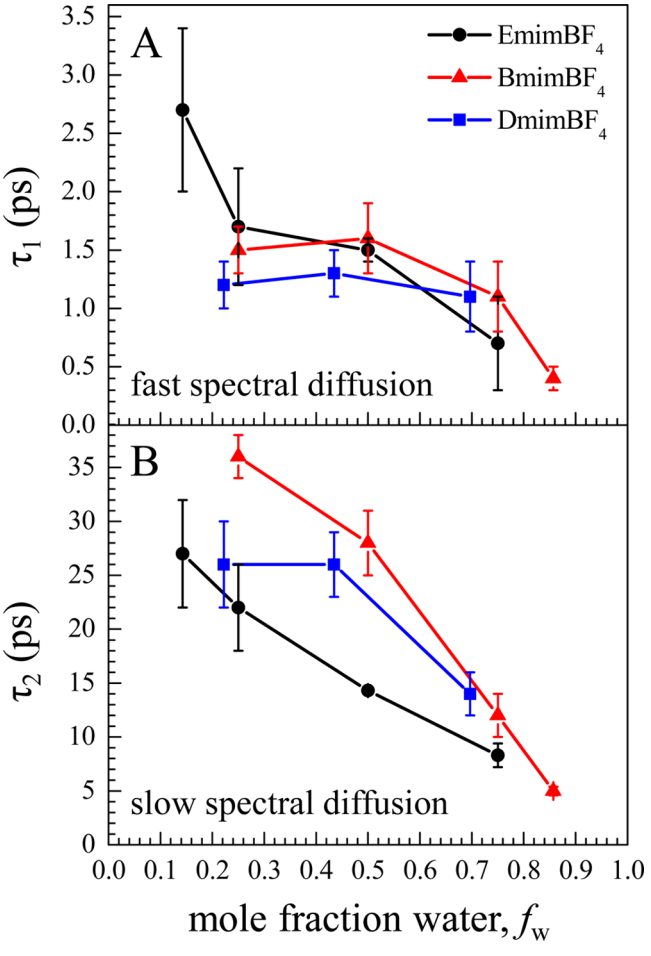

Figure 10. Spectral diffusion time constants for OD stretch of HOD in the RTIL solutions as a function of water mole fraction, f_w. (A) faster spectral diffusion time constant, τ_1; (B) slower spectral diffusion time constant, τ_2. The correspondence of mole fractions to mole ratios is given in Table 3.

In Section III.C, we found that water reorientation in $BmimBF_4$ solutions could be slower than that in IL solutions with longer or shorter alkyl chain lengths near the 1:1 ion pair to water ratio (Figure 6). From the lowest water fraction at which all three solutions were studied, 0.25, to the middle fraction of 0.5, the slower spectral diffusion component, τ_2, of the OD stretch of HOD is longer in $BmimBF_4$ solutions than in $EmimBF_4$ and $DmimBF_4$. Thus, the enhancement of alkyl chain correlations due to the increased freedom in the ionic domains, caused by water addition in a turnover-like manner,[62] is evident in water's structural dynamics at even lower water concentrations than a 1:1 ratio. Upon increasing the water concentration beyond the 0.5 water fraction, the ionic region structures in $BmimBF_4$ solutions are substantially reorganized, leading to a rapid acceleration of both structural fluctuations around the hydroxyl (Figure 10B) and water reorientation (Figure 6).

A recent study was conducted using fluorescence anisotropy measurements with a nonpolar tracer to monitor IL structural dynamics as a function of water concentration in this same homologous $BmimBF_4$ through $DmimBF_4$ series.[72] The experiments showed that for $DmimBF_4$, from no water to the point of phase separation, the alkyl region did not change structure. This is in contrast to the $BmimBF_4$ solutions, where addition of water made continuous and large structural changes to the alkyl regions as water was added. Here, the complementary 2D IR experiments show that structural modifications, as reported by water spectral diffusion, change continuously; the spectral diffusion becomes faster as water is added to the $Emim^+$ and $Bmim^+$ solutions. In contrast, the water spectral diffusion in $Dmim^+$ solutions does not change with the initial increase in water concentration. When the water concentration is increased further, the water spectral diffusion does begin to accelerate considerably, but further water addition is resisted by the alkyl chain structure. Phase separation occurs before new water arrangements can produce even faster water spectral diffusion, as is possible in the shorter chain $BmimBF_4$ and $EmimBF_4$ RTIL solutions.

IV. CONCLUDING REMARKS

The effects of water concentration and alkyl chain length on the dynamics in 1-alkyl-3-methylimidazolium tetrafluoroborate ($RmimBF_4$) RTILs have been characterized using linear FTIR, polarization-selective IR pump probe, and 2D IR vibrational echo spectroscopies to observe water's hydroxyl stretch (OD of dilute HOD in H_2O). The local environments felt by the water, as reported by the linear spectra, are fairly similar in the different RTILs studied. At low water concentrations, all hydroxyls interact only with anions. As the

DOI: 10.1021/acs.jpcb.6b08410
J. Phys. Chem. B 2016, 120, 11523−11538

water concentration is increased to ~1:1 ion pairs to water, a second population of water-associated water hydroxyls is established. In all three chain length RTILs studied with comparable water content, these two water populations exhibit nearly identical linear absorption spectra and vibrational energy relaxation lifetimes. The spectra and lifetimes report on the very local interactions between the hydroxyl (OD) its environment. Thus, the local hydrogen bonding structures are strongly conserved among ILs in this series.

The growth of hydrogen-bonded water domains is one structural modification mechanism present in the RTIL−water mixtures. As the water clusters grow, the ionic regions are disrupted and the liquid structure can be described as becoming more fluidized. Both reorientation of the hydroxyls and their spectral diffusion, tracking fluctuations in the local structures and interactions, were found to speed up noticeably with increasing water content in certain concentration ranges (Figures 6 and 10).

Independent of water content, an RTIL-ordering mechanism is the segregation of polar and nonpolar groups as the cation alkyl chain is increased from ethyl to butyl to decyl. The increasing ordering of nonpolar regions serves to limit the structural degrees of freedom possible for fluctuations within the ionic regions, which contain both water-associated and anion-associated water populations. The increased resistance to change with increasing chain length slows both the hydroxyl reorientation and structural rearrangement dynamics that allow water H-bond randomization.

We identified transition points in the two ordering or structural modification mechanisms in the RTIL−water mixture series, that is, formation of water clusters and increasing the extent of apolar domains. The water cluster ordering of the ionic regions becomes dominant for water concentrations greater than or equal to 1:1 ion pairs to water molecules, as shown by the rapid acceleration of long-time-scale spectral diffusion. For water concentrations above a mole fraction of 0.5 (Figure 10), the long-time-scale spectral diffusion is caused by structural fluctuations in the ionic region coupling to the hydroxyl. It is well established from MD simulations and scattering experiments that the chain length of $BmimBF_4$ is the shortest for which polar−apolar ordering occurs.[21,63−65] For alkyl chain lengths of four or more carbons, the water reorientation and structural randomization dynamics are found to be generally slower than those in relatively low water $EmimBF_4$ solutions (Figures 6 and 10). The sample in which both alkyl chain aggregation becomes significant and water cluster growth becomes considerable, 1:1 $BmimBF_4$ to water, is thus interesting. While water pooling is beginning to fluidize the structure and accelerate the water fluctuation dynamics in the ionic regions, the nonpolar regions are serving to restrict the ionic region motions in other ways. The alkyl region organization is actually enhanced in a narrow regime of water concentration due to disruption of the ionic region by water.[62] $BmimBF_4$ breaks the monotonic trend of slower dynamics as the chain length increases because of this unique cooperativity between the ionic region and alkyl aggregate restructuring.

The bulk viscosity is typically a poor guide to the dynamics and interactions in highly heterogeneous RTILs.[41] This work has provided information on the selective tuning of dynamics within the ionic regions of RTILs using both cation chain length modification and cosolvent (water) addition, which can be useful in a variety of RTIL applications.

AUTHOR INFORMATION

Corresponding Author

*E-mail: fayer@stanford.edu. Phone: (650) 723-4446.

Notes

The authors declare no competing financial interest.

ACKNOWLEDGMENTS

This work was funded by the Division of Chemical Sciences, Geosciences, and Biosciences, Office of Basic Energy Sciences of the U.S. Department of Energy through Grant # DE-FG03-84ER13251. P.L.K. acknowledges partial support from an ARCS fellowship.

REFERENCES

(1) Hayes, R.; Warr, G. G.; Atkin, R. Structure and Nanostructure in Ionic Liquids. *Chem. Rev.* **2015**, *115*, 6357−6426.
(2) Plechkova, N. V.; Seddon, K. R. Applications of Ionic Liquids in the Chemical Industry. *Chem. Soc. Rev.* **2008**, *37*, 123−150.
(3) Castner, E. W.; Margulis, C. J.; Maroncelli, M.; Wishart, J. F. Ionic Liquids: Structure and Photochemical Reactions. *Annu. Rev. Phys. Chem.* **2011**, *62*, 85−105.
(4) Hollenkamp, A. F.; Howlett, P. C.; MacFarlane, D. R.; Forsyth, S. A.; Forsyth, M. Energy Storage Devices. U.S. Patent 7,479,353, Jan 20, 2009.
(5) Leigang, X.; Tucker, T. G.; Angell, C. A. Ionic Liquid Redox Catholyte for High Energy Efficiency, Low-Cost Energy Storage. *Adv. Energy Mater.* **2015**, *5*, No. 1500271.
(6) Lin, M.-C.; Gong, M.; Lu, B.; Wu, Y.; Wang, D.-Y.; Guan, M.; Angell, M.; Chen, C.; Yang, J.; Hwang, B.-J.; et al. An Ultrafast Rechargeable Aluminium-Ion Battery. *Nature* **2015**, *520*, 324−328.
(7) Han, X.; Armstrong, D. W. Ionic Liquids in Separations. *Acc. Chem. Res.* **2007**, *40*, 1079−1086.
(8) Kohno, Y.; Ohno, H. Ionic Liquid/Water Mixtures: From Hostility to Conciliation. *Chem. Commun.* **2012**, *48*, 7119−7130.
(9) Zhang, X.; Zhang, X.; Dong, H.; Zhao, Z.; Zhang, S.; Huang, Y. Carbon Capture with Ionic Liquids: Overview and Progress. *Energy Environ. Sci.* **2012**, *5*, 6668−6681.
(10) Boot-Handford, M. E.; Abanades, J. C.; Anthony, E. J.; Blunt, M. J.; Brandani, S.; Mac Dowell, N.; Fernandez, J. R.; Ferrari, M.-C.; Gross, R.; Hallett, J. P.; et al. Carbon Capture and Storage Update. *Energy Environ. Sci.* **2014**, *7*, 130−189.
(11) Welton, T. Room-Temperature Ionic Liquids. Solvents for Synthesis and Catalysis. *Chem. Rev.* **1999**, *99*, 2071−2084.
(12) Hallett, J. P.; Welton, T. Room-Temperature Ionic Liquids: Solvents for Synthesis and Catalysis. 2. *Chem. Rev.* **2011**, *111*, 3508−3576.
(13) Khupse, N. D.; Kumar, A. The Cosolvent-Directed Diels-Alder Reaction in Ionic Liquids. *J. Phys. Chem. A* **2011**, *115*, 10211−10217.
(14) Kubisa, P. Ionic Liquids in the Synthesis and Modification of Polymers. *J. Polym. Sci., Part A: Polym. Chem.* **2005**, *43*, 4675−4683.
(15) Kohlmann, C.; Greiner, L.; Leitner, W.; Wandrey, C.; Luetz, S. Ionic Liquids as Performance Additives for Electroenzymatic Syntheses. *Chem. Eur. J.* **2009**, *15*, 11692−11700.
(16) Tran, C. D.; De Paoli Lacerda, S. H.; Oliveira, D. Absorption of Water by Room-Temperature Ionic Liquids: Effect of Anions on Concentration and State of Water. *Appl. Spectrosc.* **2003**, *57*, 152−157.
(17) Cammarata, L.; Kazarian, S. G.; Salter, P. A.; Welton, T. Molecular States of Water in Room Temperature Ionic Liquids. *Phys. Chem. Chem. Phys.* **2001**, *3*, 5192−5200.
(18) Khupse, N. D.; Kumar, A. Delineating Solute-Solvent Interactions in Binary Mixtures of Ionic Liquids in Molecular Solvents and Preferential Solvation Approach. *J. Phys. Chem. B* **2011**, *115*, 711−718.
(19) Ries, L. A. S.; do Amaral, F. A.; Matos, K.; Martini, E. M. A.; de Souza, M. O.; de Souza, R. F. Evidence of Change in the Molecular Organization of 1-N-Butyl-3-Methylimidazolium Tetrafluoroborate

DOI: 10.1021/acs.jpcb.6b08410
J. Phys. Chem. B 2016, 120, 11523−11538

Ionic Liquid Solutions with the Addition of Water. *Polyhedron* **2008**, *27*, 3287−3293.
(20) Sturlaugson, A. L.; Fruchey, K. S.; Fayer, M. D. Orientational Dynamics of Room Temperature Ionic Liquid/Water Mixtures: Evidence for Water-Induced Structure and Anisotropic Cation Solvation. *J. Phys. Chem. B* **2012**, *116*, 1777−1787.
(21) Canongia Lopes, J. N. A.; Pádua, A. A. H. Nanostructural Organization in Ionic Liquids. *J. Phys. Chem. B* **2006**, *110*, 3330−3335.
(22) Wang, Y.; Voth, G. A. Unique Spatial Heterogeneity in Ionic Liquids. *J. Am. Chem. Soc.* **2005**, *127*, 12192−12193.
(23) Margulis, C. J. Computational Study of Imidazolium-Based Ionic Solvents with Alkyl Substituents of Different Lengths. *Mol. Phys.* **2004**, *102*, 829−838.
(24) Triolo, A.; Russina, O.; Bleif, H.-J.; Di Cola, E. Nanoscale Segregation in Room Temperature Ionic Liquids. *J. Phys. Chem. B* **2007**, *111*, 4641−4644.
(25) Araque, J. C.; Hettige, J. J.; Margulis, C. J. Modern Room Temperature Ionic Liquids, a Simple Guide to Understanding Their Structure and How It May Relate to Dynamics. *J. Phys. Chem. B* **2015**, *119*, 12727−12740.
(26) Santos, L. M. N. B. F.; Canongia Lopes, J. N.; Coutinho, J. A. P.; Esperança, J. M. S. S.; Gomes, L. R.; Marrucho, I. M.; Rebelo, L. P. N. Ionic Liquids: First Direct Determination of Their Cohesive Energy. *J. Am. Chem. Soc.* **2007**, *129*, 284−285.
(27) Kanzaki, R.; Mitsugi, T.; Fukuda, S.; Fujii, K.; Takeuchi, M.; Soejima, Y.; Takamuku, T.; Yamaguchi, T.; Umebayashi, Y.; Ishiguro, S.-i. Ion−Ion Interaction in Room Temperature Ionic Liquid 1-Ethyl-3-Methylimidazolium Tetrafluoroborate Studied by Large Angle X-Ray Scattering Experiment and Molecular Dynamics Simulations. *J. Mol. Liq.* **2009**, *147*, 77−82.
(28) Resende Prado, C. E.; Gomide Freitas, L. C. Molecular Dynamics Simulation of the Room-Temperature Ionic Liquid 1-Butyl-3-Methylimidazolium Tetrafluoroborate. *J. Mol. Struc.: THEOCHEM* **2007**, *847*, 93−100.
(29) Izgorodina, E. I.; Golze, D.; Maganti, R.; Armel, V.; Taige, M.; Schubert, T. J. S.; MacFarlane, D. R. Importance of Dispersion Forces for Prediction of Thermodynamic and Transport Properties of Some Common Ionic Liquids. *Phys. Chem. Chem. Phys.* **2014**, *16*, 7209−7221.
(30) Liu, Z.; Huang, S.; Wang, W. A Refined Force Field for Molecular Simulation of Imidazolium-Based Ionic Liquids. *J. Phys. Chem. B* **2004**, *108*, 12978−12989.
(31) Moreno, M.; Castiglione, F.; Mele, A.; Pasqui, C.; Raos, G. Interaction of Water with the Model Ionic Liquid [Bmim][BF4]: Molecular Dynamics Simulations and Comparison with NMR Data. *J. Phys. Chem. B* **2008**, *112*, 7826−7836.
(32) Mele, A.; Tran, C. D.; De Paoli Lacerda, S. H. The Structure of a Room-Temperature Ionic Liquid with and without Trace Amounts of Water: The Role of Ch···O and Ch···F Interactions in 1-N-Butyl-3-Methylimidazolium Tetrafluoroborate. *Angew. Chem., Int. Ed.* **2003**, *42*, 4364−4366.
(33) Zhang, L.; Xu, Z.; Wang, Y.; Li, H. Prediction of the Solvation and Structural Properties of Ionic Liquids in Water by Two-Dimensional Correlation Spectroscopy. *J. Phys. Chem. B* **2008**, *112*, 6411−6419.
(34) Canongia Lopes, J. N.; Costa Gomes, M. F.; Pádua, A. A. H. Nonpolar, Polar, and Associating Solutes in Ionic Liquids. *J. Phys. Chem. B* **2006**, *110*, 16816−16818.
(35) Feng, S.; Voth, G. A. Molecular Dynamics Simulations of Imidazolium-Based Ionic Liquid/Water Mixtures: Alkyl Side Chain Length and Anion Effects. *Fluid Phase Equilib.* **2010**, *294*, 148−156.
(36) Woutersen, S.; Bakker, H. J. Resonant Intermolecular Transfer of Vibrational Energy in Liquid Water. *Nature* **1999**, *402*, 507−509.
(37) Gaffney, K. J.; Piletic, I. R.; Fayer, M. D. Orientational Relaxation and Vibrational Excitation Transfer in Methanol - Carbon Tetrachloride Solutions. *J. Chem. Phys.* **2003**, *118*, 2270−2278.
(38) Park, S.; Kwak, K.; Fayer, M. D. Ultrafast 2D-IR Vibrational Echo Spectroscopy: A Probe of Molecular Dynamics. *Laser Phys. Lett.* **2007**, *4*, 704−718.
(39) Fenn, E. E.; Wong, D. B.; Fayer, M. D. Water Dynamics in Small Reverse Micelles in Two Solvents: Two-Dimensional Infrared Vibrational Echoes with Two-Dimensional Background Subtraction. *J. Chem. Phys.* **2011**, *134*, No. 054512.
(40) Stangret, J.; Gampe, T. Ionic Hydration Behavior Derived from Infrared Spectra in HDO. *J. Phys. Chem. A* **2002**, *106*, 5393.
(41) Kramer, P. L.; Giammanco, C. H.; Fayer, M. D. Dynamics of Water, Methanol, and Ethanol in a Room Temperature Ionic Liquid. *J. Chem. Phys.* **2015**, *142*, No. 212408.
(42) Wong, D. B.; Giammanco, C. H.; Fenn, E. E.; Fayer, M. D. Dynamics of Isolated Water Molecules in a Sea of Ions in a Room Temperature Ionic Liquid. *J. Phys. Chem. B* **2013**, *117*, 623−635.
(43) Terranova, Z. L.; Corcelli, S. A. Molecular Dynamics Investigation of the Vibrational Spectroscopy of Isolated Water in an Ionic Liquid. *J. Phys. Chem. B* **2014**, *118*, 8264−8272.
(44) Corcelli, S.; Lawrence, C. P.; Skinner, J. L. Combined Electronic Structure/Molecular Dynamics Approach for Ultrafast Infrared Spectroscopy of Dilute HOD in Liquid H_2O and D_2O. *J. Chem. Phys.* **2004**, *120*, 8107−8117.
(45) Kenkre, V. M.; Tokmakoff, A.; Fayer, M. D. Theory of Vibrational Relaxation of Polyatomic Molecules in Liquids. *J. Chem. Phys.* **1994**, *101*, 10618.
(46) Schmidt, J. R.; Corcelli, S. A.; Skinner, J. L. Pronounced Non-Condon Effects in the Ultrafast Infrared Spectroscopy of Water. *J. Chem. Phys.* **2005**, *123*, No. 044513.
(47) Moilanen, D. E.; Fenn, E. E.; Lin, Y. S.; Skinner, J. L.; Bagchi, B.; Fayer, M. D. Water Inertial Reorientation: Hydrogen Bond Strength and the Angular Potential. *Proc. Natl. Acad. Sci. U.S.A.* **2008**, *105*, 5295−5300.
(48) Lipari, G.; Szabo, A. Effect of Librational Motion on Fluorescence Depolarization and Nuclear Magnetic-Resonance Relaxation in Macromolecules and Membranes. *Biophys. J.* **1980**, *30*, 489−506.
(49) Kinosita, K.; Ikegami, A.; Kawato, S. On the Wobbling-in-Cone Analysis of Fluorescence Anisotropy Decay. *Biophys. J.* **1982**, *37*, 461−464.
(50) Kinosita, K.; Kawato, S.; Ikegami, A. Theory of Fluorescence Polarization Decay in Membranes. *Biophys. J.* **1977**, *20*, 289−305.
(51) Moilanen, D. E.; Fenn, E. E.; Wong, D.; Fayer, M. D. Water Dynamics in Large and Small Reverse Micelles: From Two Ensembles to Collective Behavior. *J. Chem. Phys.* **2009**, *131*, No. 014704.
(52) Park, S.; Moilanen, D. E.; Fayer, M. D. Water Dynamics-the Effects of Ions and Nanoconfinement. *J. Phys. Chem. B* **2008**, *112*, 5279−5290.
(53) Rezus, Y. L. A.; Bakker, H. J. On the Orientational Relaxation of HDO in Liquid Water. *J. Chem. Phys.* **2005**, *123*, No. 114502.
(54) Moilanen, D. E.; Piletic, I. R.; Fayer, M. D. Water Dynamics in Nafion Fuel Cell Membranes: The Effects of Confinement and Structural Changes on the Hydrogen Bonding Network. *J. Phys. Chem. C* **2007**, *111*, 8884−8891.
(55) Giammanco, C. H.; Wong, D. B.; Fayer, M. D. Water Dynamics in Divalent and Monovalent Concentrated Salt Solutions. *J. Phys. Chem. B* **2012**, *116*, 13781−13792.
(56) Rezus, Y. L. A.; Bakker, H. J. Strong Slowing Down of Water Reorientation in Mixtures of Water and Tetramethylurea. *J. Phys. Chem. A* **2008**, *112*, 2355−2361.
(57) Laage, D.; Hynes, J. T. A Molecular Jump Mechanism of Water Reorientation. *Science* **2006**, *311*, 832−835.
(58) Laage, D.; Hynes, J. T. On the Molecular Mechanism of Water Reorientation. *J. Phys. Chem. B* **2008**, *112*, 14230−14242.
(59) Tan, H.-S.; Piletic, I. R.; Fayer, M. D. Orientational Dynamics of Water Confined on a Nanometer Length Scale in Reverse Micelles. *J. Chem. Phys.* **2005**, *122*, No. 174501.
(60) Laage, D.; Stirnemann, G.; Hynes, J. T. Why Water Reorientation Slows without Iceberg Formation around Hydrophobic Solutes. *J. Phys. Chem. B* **2009**, *113*, 2428−2435.
(61) Canongia Lopes, J. N.; Pádua, A. A. H. Molecular Force Field for Ionic Liquids III: Imidazolium, Pyridinium, and Phosphonium

DOI: 10.1021/acs.jpcb.6b08410
J. Phys. Chem. B 2016, 120, 11523−11538

Cations; Chloride, Bromide, and Dicyanamide Anions. *J. Phys. Chem. B* **2006**, *110*, 19586−19592.
(62) Jiang, W.; Wang, Y.; Voth, G. A. Molecular Dynamics Simulation of Nanostructural Organization in Ionic Liquid/Water Mixtures. *J. Phys. Chem. B* **2007**, *111*, 4812−4818.
(63) Shimizu, K.; Bernardes, C. E. S.; Canongia Lopes, J. N. Structure and Aggregation in the 1-Alkyl-3-Methylimidazolium Bis-(Trifluoromethylsulfonyl)Imide Ionic Liquid Homologous Series. *J. Phys. Chem. B* **2014**, *118*, 567−576.
(64) Rocha, M. A. A.; Lima, C. F. R. A. C.; Gomes, L. R.; Schröder, B.; Coutinho, J. A. P.; Marrucho, I. M.; Esperança, J. M. S. S.; Rebelo, L. P. N.; Shimizu, K.; Lopes, J. N. C.; et al. High-Accuracy Vapor Pressure Data of the Extended [Cnc1im][Ntf2] Ionic Liquid Series: Trend Changes and Structural Shifts. *J. Phys. Chem. B* **2011**, *115*, 10919−10926.
(65) Rocha, M. A. A.; Neves, C. M. S. S.; Freire, M. G.; Russina, O.; Triolo, A.; Coutinho, J. A. P.; Santos, L. M. N. B. F. Alkylimidazolium Based Ionic Liquids: Impact of Cation Symmetry on Their Nanoscale Structural Organization. *J. Phys. Chem. B* **2013**, *117*, 10889−10897.
(66) Kwak, K.; Rosenfeld, D. E.; Fayer, M. D. Taking Apart the Two-Dimensional Infrared Vibrational Echo Spectra: More Information and Elimination of Distortions. *J. Chem. Phys.* **2008**, *128*, No. 204505.
(67) Kwak, K.; Park, S.; Finkelstein, I. J.; Fayer, M. D. Frequency-Frequency Correlation Functions and Apodization in Two-Dimensional Infrared Vibrational Echo Spectroscopy: A New Approach. *J. Chem. Phys.* **2007**, *127*, No. 124503.
(68) Park, S.; Fayer, M. D. Hydrogen Bond Dynamics in Aqueous NaBr Solutions. *Proc. Natl. Acad. Sci. U.S.A.* **2007**, *104*, 16731−16738.
(69) Tamimi, A.; Bailey, H. E.; Fayer, M. D. Alkyl Chain Length Dependence of the Dynamics and Structure in the Ionic Regions of Room-Temperature Ionic Liquids. *J. Phys. Chem. B* **2016**, *120*, 7488−7501.
(70) Sturlaugson, A. L.; Arima, A. Y.; Bailey, H. E.; Fayer, M. D. Orientational Dynamics in a Lyotropic Room Temperature Ionic Liquid. *J. Phys. Chem. B* **2013**, *117*, 14775−14784.
(71) Asbury, J. B.; Steinel, T.; Stromberg, C.; Corcelli, S. A.; Lawrence, C. P.; Skinner, J. L.; Fayer, M. D. Water Dynamics: Vibrational Echo Correlation Spectroscopy and Comparison to Molecular Dynamics Simulations. *J. Phys. Chem. A* **2004**, *108*, 1107−1119.
(72) Thomaz, J. E.; Lawler, C. M.; Fayer, M. D. The Influence of Water on the Alkyl Region Structure in Variable Chain Length Imidazolium-Based Ionic Liquid/Water Mixtures. *J. Phys. Chem. B* **2016**, *120*, 10350−10357.

DOI: 10.1021/acs.jpcb.6b08410
J. Phys. Chem. B 2016, 120, 11523−11538